Meteorol. Z. (Contrib. Atm. Sci.), Vol. **32**, No. 4, 293–315 (published online July 6, 2023)

Meteorological and air quality measurements in a city region with complex terrain: influence of meteorological phenomena on urban climate

Abdul Samad[1*], Olga Kiseleva[2], Christopher Claus Holst[3], Robert Wegener[4], Meinolf Kossmann[5], Gregor Meusel[6], Alina Fiehn[7], Thilo Erbertseder[8], Ralf Becker[9], Anke Roiger[7], Peter Stanislawsky[5], Dieter Klemp[4], Stefan Emeis[3], Norbert Kalthoff[2] and Ulrich Vogt[1]

[1]Institute of Combustion and Power Plant Technology (IFK), University of Stuttgart, Stuttgart, Germany
[2]Institute of Meteorology and Climate Research –Troposphere Research (IMK-TRO), Karlsruhe Institute of Technology(KIT), Karlsruhe, Germany
[3]Institute of Meteorology and Climate Research – Atmospheric Environmental Research (IMK-IFU), Karlsruhe Institute of Technology (KIT), Garmisch-Partenkirchen, Germany
[4]Institute of Energy and Climate Research (IEK8: Troposphere), Forschungszentrum Jülich GmbH (FZJ), Jülich, Germany
[5]Department of Climate and Environment Consultancy (KU1), German Meteorological Service (DWD), Offenbach/Potsdam, Germany
[6]Institute of Meteorology and Climatology (IMUK), Leibniz University Hannover, Hannover, Germany (LUH), Hannover, Germany
[7]Institute of Atmospheric Physics, German Aerospace Center (DLR), Oberpfaffenhofen, Germany
[8]German Remote Sensing Data Center (DFD), German Aerospace Center (DLR), Oberpfaffenhofen, Germany
[9]Lindenberg Meteorological Observatory (MOL), German Meteorological Service (DWD), Germany

(Manuscript received January 9, 2022; in revised form January 19, 2023; accepted February 20, 2023)

Abstract

On 8 and 9 July 2018 extensive observations were conducted under fair-weather conditions in the German city of Stuttgart and its surroundings. This intensive observation period, part of the four weeks Urban Climate Under Change $(UC)^2$ campaign, intended to provide a comprehensive data set to understand the complex interactions of thermally induced wind systems, vertical turbulent mixing and air pollutant concentration distribution in the atmospheric boundary layer of the city. Stuttgart has a very special and complex topography with a city center located in a basin surrounded by 250 to 300 m higher hills influencing the wind and flow system, reducing the wind speed, and causing inhibited dispersion of air pollutants. Cold air flows from the surrounding plains can penetrate the urban areas and influence the urban climate including the air quality. For investigating these effects with a focus on urban climate, combinations of different measurement platforms and techniques were used, such as in situ stationary and mobile measurements with cars, vertical profiling by means of tethered balloons, radiosondes, a drone, and aircraft observations, remote sensing devices and satellite-based instruments. Numerous atmospheric processes in an urban area regarding boundary layer evolution, inversion, local wind systems, urban heat island, etc. were observed. Some important findings are: Temperature observations provide local information about the warmest areas in the city and about the city and its surroundings. The urban heat island effect was evident from the results of stationary and mobile air temperature measurements as the higher air temperature was measured in the Stuttgart basin compared to its surroundings. Considerable spatio-temporal differences concerning the wind (speed and direction), turbulence and the convective boundary depth are evident. Lower wind speeds were observed during the nighttime and the main wind direction in the Stuttgart valley was measured to be southwest, which carried cold air from the hillsides into the city and pollutants to the windward side of the city into the Neckar valley. The low wind speed favored the accumulation of pollutants in a shallow nocturnal boundary layer close to the surface. During the day, the overall pollutant concentration was reduced by vertical convective mixing. The vertical profile measurements have shown that the applied techniques provided a good overview to understand the vertical characteristics of meteorological parameters and pollutants as well as the stability of the atmosphere and extent of the urban boundary layer. It also showed that the extent of atmospheric mixing determines the dispersion, dilution and mixing of emitted pollutants.

Finally, the additional comprehensive air-chemical observations (surface and satellite based) allow an understanding of the diurnal cycle of air pollutants in the atmospheric boundary layer of the city of Stuttgart. Satellite-based observations from Sentinel-5P/TROPOMI have shown their potential for mapping urban pollution islands and urban pollution plumes even in cities with a complex terrain like Stuttgart. These observations assisted to obtain a comprehensive data set intended for the validation of a novel urban climate model, PALM-4U.

Keywords: Urban atmospheric processes, urban climate, urban boundary layer, temperature inversion, vertical profiles, thermal wind systems, topography, air pollutants, tethered balloon measurements, drone measurements, radiosonde measurements, airplane measurements, mobile measurements, satellite measurements

*Corresponding author: Abdul Samad, Institute of Combustion and Power Plant Technology (IFK), University of Stuttgart, Stuttgart, Pfaffenwaldring 23, 70569 Stuttgart, Germany, e-mail: abdul.samad@ifk.uni-stuttgart.de

DOI 10.1127/metz/2023/1124
Gebrüder Borntraeger Science Publishers, Stuttgart, www.borntraeger-cramer.com

1 Introduction

Urban climate has been a burning issue for many decades now and it is becoming more and more relevant. Questions like the impact of air quality on the urban population are the subject of investigations. Urban climate models are a useful tool, that can be applied to simulate scenarios of various complexity in urban environments (Milner et al., 2019), for example air quality studies in street canyons. However, these models need to be validated with the help of actual measurement results. Usually, meteorology and air quality are measured by stationary monitoring stations, at well-defined heights above the surface and with certain averaging intervals. However, these data lack spatial coverage, which limits the understanding of complex 3D processes related to urban climate. In order to provide high spatial and temporal resolution data for meteorology and air quality, three-dimensional measurements are essential. The use of mobile measurement platforms can fill the lack of spatial measurement data. They were successfully operated in different research projects in the past (Bukowiecki et al., 2002; Ehlers, 2013; Klemp et al., 2020; Weijers et al., 2004; Westerdahl et al., 2005). These measurements assist in investigating meteorological phenomena such as boundary layer evolution, formation and dissolving of inversions, cold air flows, etc. These phenomena directly affect air quality and urban climate.

Any substance that changes the natural composition of the air is considered a pollutant (Baumbach, 1996). Air pollution is an important environmental and social problem, which is influenced by meteorological processes. The quality of air is deteriorating with an increase in anthropogenic and natural activities emitting air pollutants (European Environment Agency, 2016). Air quality in Europe is improving, however, air quality is still worse in the densely urbanized cities compared to rural areas. Urban areas with high population, dense building structures and high traffic volume face problems related to urban climate and ambient air quality. Various studies (Kampa and Castanas, 2008; Mabahwi et al., 2014) have shown that air pollution has significant adverse effects on human health and the environment. According to the World Health Organization (WHO, 2021), around 4.2 million people die every year due to ambient air pollution. These problems are directly related to the amount of emitted air pollutants, but also to meteorological conditions in the investigated area. Therefore, it is essential to understand the air quality and meteorological situation at the same time, which changes dynamically in the lowest layers of the atmosphere (Baumbach, 1996).

The stability of the atmosphere can be assessed by wind speed, solar radiation (Zoras et al., 2006) and Richardson number averaged over the surface layer (Kolev et al., 2000). In this study, the standard deviation of the vertical wind speed $\sigma(w)$ was used for the interpretation of the stability of the atmosphere. Several studies investigated the relationship between meteorology and air quality. The results of these studies show that high pollutant concentrations in the ambient air depend on factors like source strength, direction and distance of nearby emission sources etc., but it also strongly depends on the existence, duration, strength and vertical extension of stable meteorological conditions. Stable meteorological conditions can be observed, among others, during high pressure conditions when temperature inversions are developed in cities and plain sites (Janhall et al., 2006; Baumbach and Vogt, 2003) as well as in valleys (Silva et al., 2007; Olofson et al., 2009; Guzmán-Torres et al., 2009; Panday and Prinn, 2009; Schnitzhofer et al., 2009). The inversion acts as a barrier for convective processes limiting the dispersion of air pollutants by preventing vertical and horizontal mixing (Baumbach, 1996; Faragó et al., 2005). Typically, surface inversions are formed due to the cooling of the air masses that are close to the earth's surface at night. The cooling of the air masses is caused by the cooling of the earth's surface by energy loss in the IR range due to the absence of low clouds during night-time. The development of a strong inversion is favored by low wind speeds, clear skies along with longer and colder nights whereas heat which is absorbed in buildings structures or other surfaces of urban agglomerations, and which is released during nighttime, counteract the formation of stable stratification (Britannica, 2020). Since the nighttime in winter is longer than in summer, therefore stronger inversions, related to the temperature difference between the lower boundary and the upper boundary of the temperature inversion as well as to its vertical extension, usually occur during the wintertime. During the daytime, such a surface inversion gradually weakens and disappears as solar radiation gradually warms up the surface. Local topographical structures can influence the development of inversions like in valleys (Baumbach, 1996). Strong inversions are also observed in Stuttgart during clear nights in summer (Kiseleva et al., 2022). Local wind systems, even with low wind speeds, play an important role in the aeration of an area (Vogt et al., 1999) These local wind systems are formed in valleys and at slopes because of the change in air temperature, air pressure and shielding effect of the surrounding mountain ranges. Fig. 1(b) shows the topographical situation of Stuttgart's city basin, consisting of Nesenbach valley and the west basin (Baumüller et al., 1998). These two parts are separated by a ledge, which forms the southern border of the wind-sheltered west basin. The ledge channels the wind flow in the Nesenbach valley, towards the city center. This causes an increase in the speed, the vertical extension and the volume streams of the airflow through the Nesenbach valley. The ridge, which divides parallel the Feuerbach valley and Stuttgart's city basin, also affects the climate. Fig. 1(c) shows the results of a simulation performed for the cold airflows and the distribution of wind speeds

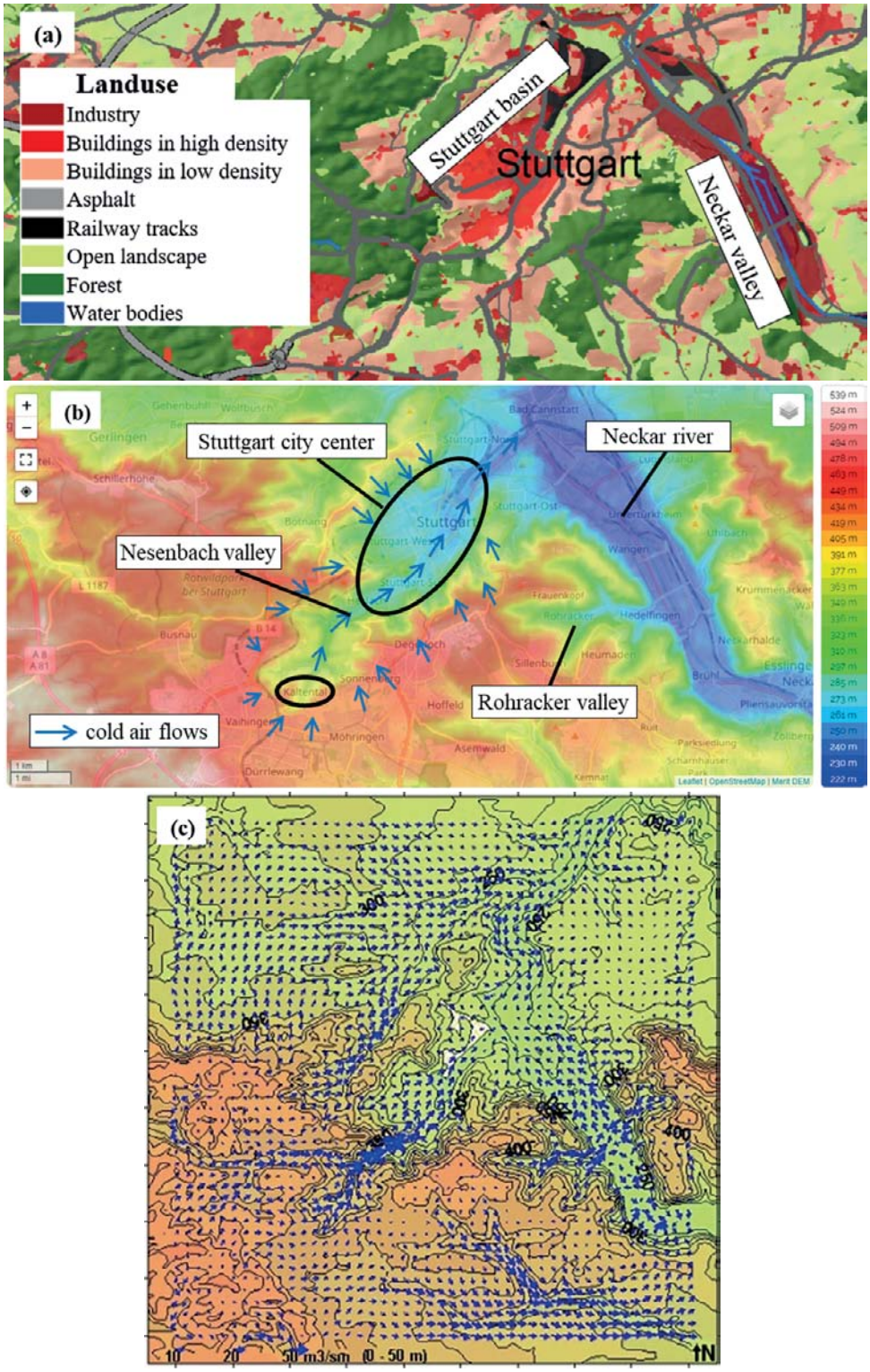

Figure 1: (a) to (c): a) Landuse map of Stuttgart (Baumüller, 2008). b) Topographic map of Stuttgart (Yamazaki et al., 2017), source: OpenStreetMap. c) results of a cold airflow simulation in Stuttgart (Schädler and Lohmeyer, 1996)

in Stuttgart's basin valley. The maximum wind speed is 3 m/s with the highest wind speeds reached at Nesenbach valley and Rohracker valley. However, the amount of cold air is more crucial than the wind speed in this situation. Since all valleys are cold air catchment areas, it can be seen that the volume flow density is higher at valleys (Schädler and Lohmeyer, 1996).

An urban climate model with a high spatial resolution that can resolve local information such as buildings, street canyons, etc. as well as entire city regions can assist the community to cope with urban climate concerns. Such a model is developed in a German research programm "Urban Climate Under Change" $[UC]^2$ (Scherer et al., 2019a). In this research

programm, three-dimensional observation data are obtained for model validation as well as testing its practicability so that it can be used in the scientific world with confidence. The planning authorities need comprehensive information on urban atmospheric processes with high spatial resolution data in order to predict future climatic conditions. Hence, building-resolving urban climate models for entire city regions play an important role in urban development and planning, air quality control, as well as the approaches to address the climate change issues (Scherer et al., 2019a). Three-dimensional observation data are acquired for model validation through the research institutes in the group named "Three-dimensional Observation of Atmospheric Processes in Cities" (3DO) (Scherer et al., 2019b). This group collected accurate three-dimensional observational data sets on meteorology and air quality in the German cities of Berlin, Hamburg and Stuttgart, which are used for the evaluation of the new urban climate model called PALM-4U (Maronga et al., 2020). PALM-4U also contains modules to simulate air quality (Khan et al., 2021). Apart from validating this urban climate model, the individual urban atmospheric processes can also be investigated from the measured data, spatio-temporal evolution of urban boundary layer and air quality and can be used as input for urban climate planning maps (identification ventilation paths and of hot spots, i.e. quarters with high heat load or poor air quality). These measurement data were obtained with Long Term Observations (LTO) as well as with intensive measurements performed during Intensive Observation Periods (IOP). During 3DO four IOPs were performed in Stuttgart during the summer and winter of 2017 and 2018. The IOP days were selected based on low cloud cover (less than 5/8), weak regional winds (<3 m/s at Stuttgart airport), no precipitation and no fog to obtain a data set that could help to validate a typical summer or winter day simulated with PALM-4U. The IOP selected for this study focuses on the assessment of different atmospheric processes and took place on 8 and 9 July 2018 in Stuttgart. The authors want to point out the versatility of different measurement approaches that were used to generate the data set during the IOP and that can be used to investigate numerous phenomena occurring in the city.

In the following the measurement area is presented (Section 2). The observational strategy is outlined (Section 3) and the results of one IOP are presented (Section 4). The analysis includes the investigation of thermal wind systems, boundary layer formation and height as well as the correlation of the boundary layer conditions to the air quality of the city. Different institutions performed surface-based measurements in the boundary layer, using different methodologies and measurement techniques. Additionally, satellite and aircraft-based observations help to understand the three-dimensional evolution of meteorological and air-chemical conditions in the urban boundary layer.

2 Measurement area

The city of Stuttgart is the capital of the state of Baden-Württemberg in Germany, which is the sixth largest city in Germany with a population of around 630,000 (United Nations, 2018). The city is known for its unique topography in a basin connected to the valley of river Neckar. Stuttgart is characterized by low wind speeds resulting in higher pollutant concentrations (Baumüller et al., 1998) and thus makes it interesting to study the effects of pollutant dispersion on the one side and the establishment of local wind systems on the other side. The inner city of Stuttgart is located in a valley that extends from Kaltental in the south to the river Neckar in the north (Fig. 1). The basin position determines the meteorological situation in Stuttgart as the air is channelled. While in the Neckar valley north of Stuttgart northwesterly and southeasterly winds predominate, the main wind direction within the Stuttgart valley is southwest. Cold air flows from the hills to supply the city with fresh air (clean and cold) at night. Slope winds in the morning hours transport the city's pollution to the suburban areas and the outskirts. The meteorological and urban climatic situation of Stuttgart is quite complex and special, due to the fact that the city center is situated in a basin, surrounded by hills and only opened to the northwesterly direction to the valley of the river Neckar. Caused or intensified by this special topography, local flow and wind systems are established, having their influence on the urban climate and even partly counteract each other, e.g. the valleys support the formation of temperature inversion, which leads to more stable atmospheric conditions with worse dispersion conditions, but at the same time the topography causes the transport of cold air, which can be fresh and clean air, into the city, improving the air quality there. Stuttgart is not the only city in Germany with such a topographical situation, Aachen and to a certain extent Augsburg are comparable, but in Stuttgart it is quite distinctive.

The meteorological conditions on the measurement days were these of a typical summer day in Stuttgart with dry conditions, cloud coverage less than 5/8, average near-surface wind speed lower than 3 m/s and maximum temperature reached during the day was greater than 25 °C. During the measurement campaign there was high pressure west of the British Isles and low pressure over Scandinavia generated a weak to moderate large-scale flow from northwesterly to northerly directions in the study area.

3 Measurement strategy and measurement technique

To investigate the three-dimensional atmospheric situation in the city, diverse methods and measurement techniques were applied. The various measurement methods applied can be categorized as follows:

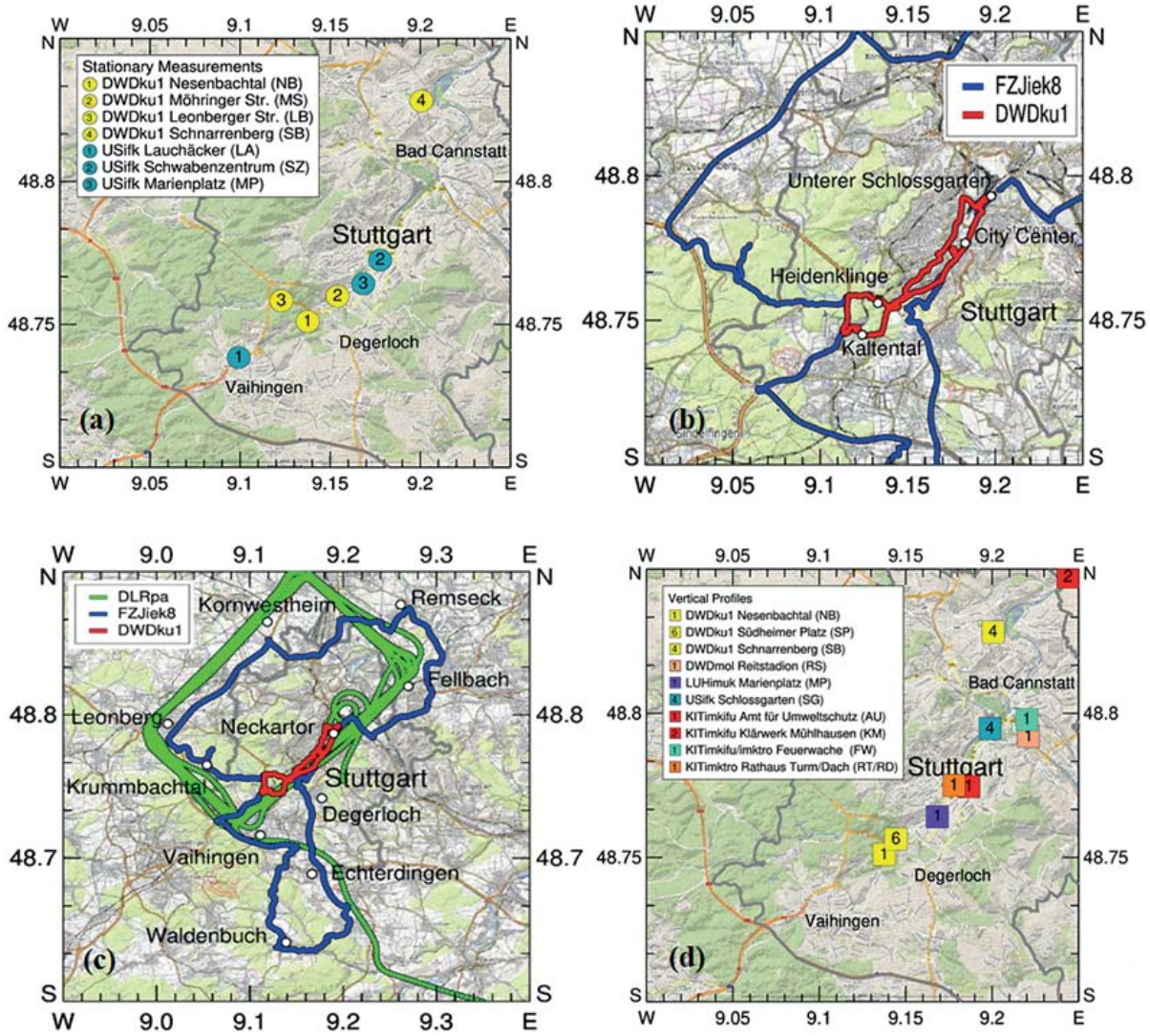

Figure 2: (a) to (d): a) Stationary measurement locations for the groups DWDku1 (yellow circles) and USifk (blue circles) during the measurement campaign. b) Mobile measurement route for the groups FZJiek8 (blue line) and DWDku1 (red line) during the measurement campaign. c) Aircraft measurement route (green line) for the group DLRpa during the measurement campaign plus routes of MobiLab from FZJiek8 (blue line) and measurement car from DWDku1 (red line). d) Vertical profile measurement locations for the groups DWDku1, LUHimuk, USifk, KITimktro and KITimkifu during the measurement campaign. For acronyms see Table 1.

- Stationary measurements – S: These measurements include the results from the stationary monitoring stations for air quality and meteorological parameters.
- Mobile measurements – M (by car and aircraft): These measurements provided information regarding the horizontal, and in the case of aircraft observations, also vertical distribution of measured parameters.
- Vertical profiles – V: The information regarding the vertical distribution of measured parameters were obtained using tethered balloons, radiosonde, SODAR, drone and Lidar systems.
- Satellite measurements – Sat: The satellite data helped to investigate the distribution of investigated parameters over the whole region to obtain a broader picture and vertically integrated quantities.

The parameters measured and the instruments used by different institutions are compiled in Table 1 and were extracted from the publication "Three-Dimensional Observation of Atmospheric Processes in Cities" (Scherer et al., 2019b).

3.1 Stationary measurements

Stationary measurements offer comprehensive information at a fixed location with high (1 s) to moderate (10 min) temporal resolution. The stations, equipped with instruments measuring meteorological parameters were positioned alongside the valley corresponding to the path of the main cold air flows from its origin Vaihingen in the south to Bad Cannstatt in the north, where they flow into the valley of the river Neckar. The stationary meteorological stations were installed

Table 1: List of instrumentation, institutions (abbreviations see author's institute information), platforms, measured parameters, measurement height, temporal resolution, type of measurements and location according to Fig. 2d.

Instrumentation	Institution	Platform	Parameters	Height	Time res.	Type	Location. Fig. 2–4
– Chemiluminescence of generated NO_2 (Eco-Physics), NO_2 photolytic converter + chemiluminescence of NO_2 (Eco-Physics), O_3 titration with excess NO + chemiluminescence of NO_2 (Eco-Physics modified) – CO resonance fluorescence (Aero laser), – NO_2 cavity attenuated phase shift (Aerodyne) – HCHO IR cavity ringdown (Picarro), CH_4, N_2O IR-ICOS laser absorption (LosGatos) – O_3 sensor (Ansyco 41M) – SO_2 sensor (Thermo Fisher TE 43i) – VOC canister sampling (Restec), GC-MS (Agilent) – Electrical low-pressure impactor (Dekati) – CPC-3788 (TSI) – Meteorology instrument (Vaisala HMT 330) – GPS (Wintec WBT202)	FZJiek8	Car	NO, NO_2, O_3 CO, CO_2, CH_4, H_2O, N_2O, NH_3 SO_2 HCHO C_2-C_{12} HC, OVOC $N_{0.006–10}$ T, U, u, v, x, y	2 m above ground	1–2 s all parameters, except for VOC sampling: 10 minutes	M	mobile
– Ceilometer (Vaisala CL51) – Wind LIDAR (Halo Photonics Streamline XR) – 2 Wind LIDAR (Halo Photonics Streamline)	KITimkifu	Roof	β, N_{al}, h_{al}, h_{cl}, c_{cl} u, v, w	40 to 2.000 m 60 to 1400 m		V	RD FW AU / KM
– Wind LIDAR (Leosphere Windcube WLS 8) – Microwave radiometer (Radiometer Physics HATPRO RPG) – Wind LIDARe Leosphere WLS 200))	KITimktro	Roof Roof Ground	u, v T, absolute humidity u, v	40 to 600 m 0 to 10 km 0 to 350 m	600 s 900 s 600 s	V	RD RT FW
– Condensation particle counter (TSI 3007) – optical particle counter (Grimm 1.108) – NO_2/NO/NO_X sensor (2B Technologies 405 nm) – O_3 sensor (2B Technologies OM202) – aethalometer (AethLabs AE51) – meteorological instrument (Kroneis) – Optical particle counter (Grimm EDM180), NO/NO*x* sensor (MLU 200A), CO sensor (Horiba APMA 360), O_3 sensor (Horiba APOA 360), aethalometer (Magee AE33), wind monitor (Lufft WS200-UMB), meteorological instrument (Lufft WS301-UMB), tipping bucket rain gauge (Lambrecht 8353.12H)	USifk	Tethered balloon Ground	N, $PM_{0.3–20}$, $N_{0.3–20}$, NO_2, NO, NO_X, O_3, BC, T, U, p, u, v PM_{10}, $PM_{0.25–32}$, $N_{0.25-32}$, NO, NO_X, NO_2, CO, O_3, BC, u, v, T, U, p, $E_{sw,d}$, P	0 to 470 m 3 m, Wind at 10 m	1 s 1 s	V S	SG MP
– SODAR (METEK) – Frankenberger psychrometer (Friedrichs T3010), temperature sensor (Hettstedt MWT PT100), humidity sensor (E+E Elektronik EE33), air pressure sensor (Druck Limited DPI261) – Radiosonde (Vaisala RS92) – Tethered balloon sondes (Vaisala DigiCORA system), pyranometer (Kipp & Zonen CM21), pyrgeometer (Kipp & Zonen CG4) – Wind monitor (Gill Solent), Temperature and humidity sensor (Vaisala HMP45d), four-component radiometer (Kipp & Zonen CNR4), weighing precipitation bucket (Ott Pluvio), wind speed sensor (Thies 4.3303.22.000), wind vane (Thies 4.3120.22.002)	DWDku1 DWDmol	Trailer Car Balloon Tethered balloon Ground	u, v, w T, U, p $E_{sw,d}$, $E_{sw,u}$, $E_{lw,d}$, $E_{lw,u}$ T, U, u, v, $E_{sw,d}$, $E_{sw,u}$, $E_{lw,d}$, $E_{lw,u}$, P	30 to 300 m 2 m 0 to 15 km 0 to 300 m 1 m 1 m, 2 m, 1 to 10 m		V M V V S	NB SP / SB NB / MS / LB / SB
Hexacopter (DJI Flamewheel550), radiosonde (GRAW DFM-06), GPS, camera (GoPro Hero 4 silver), thermal IR camera (FLIR Tau 2 640/09 mm fully radiometric + TeAx ThermalCapture 2.0)	LUHimuk	UAS	T, U, p, u, v, x, y, T_b,	0 to 300 m		V	MP
Open-wire PT100 (custom-made), absolute/differential pressure transducer (PMP 4100), capacitive humidity sensor (Vaisala Humicap HMP230), dewpoint mirror (Meteolabor TP3-S modified by DLR), Ly-alpha absorption hygrometer (Buck research L5) Dual quantencascade laser (Aerodyne), cavity attenuated phase shift NO_2 (Aerodyne), UV absorption (2B Technologies)	DLRpa	Aircraft	T, U, p, u, v, w, x, y, z CO, CO_2, C_2H_6, O_3, CH_4, NO_2, N_2O	0.15 to 6 km		V/M	
Sentinel-5P/TROPOMI	DLRdfd	Satellite	CO, CH_2O, CH_4, NO_2, O_3, SO_2	0 to 12 km		V/S	

in Nesenbach valley (NB) in the suburb Kaltental, Möhringer Str. (MS) the suburb Heslach Süd and at a higher terrain elevation Leonberger Str. (LB). An existing meteorological station is permanently in operation at Schnarrenberg (SB) for decades. A monitoring station, equipped with meteorological sensors and air quality measurement instruments at Marienplatz (MP), was also used for this campaign. Apart from that data from other stationary monitoring stations such as Lauchäcker (LA) operated by USifk and Schwabenzentrum (SZ) near the city center operated by the municipality of Stuttgart was utilized. All these measurement locations are shown in Fig. 2a and further details can be found in Table 1.

3.2 Mobile measurements

Mobile measurements provide an overview of the varying meteorological parameters and the spatial distribution of pollutants within the valley and the outflow of pollutants out of the valley. Urban heat island effects and cold air flows were studied with mobile measurements in the city and at the slopes where the cold air enters the city. The meteorological measurements by DWDku1 focused on the valley entrance at Kaltental, where the main cold airflow can be investigated, and in the city center. The data obtained consisted of transects of instantaneous near surface air temperature and humidity in 4-hour intervals from the suburb Kaltental along the Nesenbach valley and the tributary Heidenklinge via Stuttgart city center to the Unterer Schlossgarten. The route of DWDku1 is highlighted in red color in Fig. 2a.

The aim of the measurements from FZJiek8 was to quantify the emissions of Stuttgart by measuring the incoming air windward and the outflow of pollutants leeward of the valley. Therefore, MobiLab, the mobile laboratory, circumnavigated the basin of Stuttgart. The measurement route shown in Fig. 2b in blue colour started in the inner city and led northwards along the Stuttgart valley via Neckartor and Fellbach to Remseck at the river Neckar. Here the Neckar valley was left and the van returned via Kornwestheim and Leonberg to a forest site at Krummbachtal, a valley west of Stuttgart where background air free of emissions from Stuttgart was sampled. From there MobiLab went to the south via Vaihingen to Waldenbuch at the hill range in the south. The route was completed descending into the valley again from Degerloch. The whole cycle took about 150 minutes and was repeated three times a day. The route was planned to avoid highly-trafficked streets, however, from Kornwestheim to Leonberg and from Krummbachtal to Vaihingen a motorway had to be used. MobiLab is equipped with instrumentation to study the distribution of pollutants (e.g., NO, NO_2, CO, O_3, SO_2), greenhouse gases (e.g., CO_2, CH_4N_2O), aerosol number and size distribution and meteorological parameters (Klemp et al., 2020; Klemp et al., 2021). The measurements were done at 2 m above ground at a time resolution of 1 s. Details of the instrumentation can be found in Table 1.

Aircraft-borne in-situ measurements were carried out by DLRpa with a Cessna Grand Caravan airplane to study the properties of the urban boundary layer in the horizontal and vertical. In addition to meteorological parameters (air temperature, relative humidity, air pressure, wind speed and direction), distributions of greenhouse gases (CO_2, CH_4) and air pollutants (CO, NO_2, O_3) were measured in the urban boundary layer. The aircraft observations documented the evolution of the polluted boundary layer in the Stuttgart basin during the intensive measurement campaign. A total of four mission flights were executed during the campaign days (one morning and afternoon flight on both campaign days). The route of the airplane measurements which corresponds to the northern part of the route of FZJiek8 is shown in green colour in Fig. 2c.

3.3 Vertical profiles

The wind profiles are helpful to investigate atmospheric turbulence and the horizontal and vertical transport of air masses. The potential temperature results assist to inspect the boundary layer and determine temperature inversion layers (Bolton, 1980). The meteorological and air quality measurements were performed at different heights, which captured the atmospheric situation above Stuttgart in three dimensions. The measurement locations of all vertical profile measurements are shown in Fig. 2d.

Vertical profiles of meteorological parameters were measured by DWDku1 with the help of SODAR in NB near Kaltental 305 m above sea level (asl), radiosonde at Südheimer Platz (SP) valley site southwest of the city center 297 m asl, and at SB hilltop site near Neckar valley 323 m asl, and by tethersonde at Reitstadion (RS) Neckar valley site 200 m asl.

The LUHimuk group performed vertical profiles for meteorological parameters to a maximum height of 300 m above ground level (agl) at MP with the help of a radiosonde on a hexacopter (Fig. 2d) which was attached 5 m below the drone to lessen downwash effects of the rotor blades. Wind information was derived using the drifting method, where the drone is manually switched to the non-GPS-stabilized ATTI mode, whereby it is moved horizontally by the prevailing wind. The wind velocities and directions were calculated using differences in latitude and longitude.

USifk performed vertical profiles of meteorological and air quality parameters with the aid of a tethered balloon. These measurements were performed at Schlossgarten (SG) continuously during the whole campaign.

The remote sensing systems of KITimktro included one Doppler wind Lidar (Windcube), one scanning microwave radiometer of type HATPRO RPG (MWR) (for details see Kalthoff et al., 2013, dataset in Kiseleva et al., 2019) and three Doppler wind Lidars WLS200 (Table 1). The Windcube and the MWR were placed on the rooftops of two buildings of the town hall (Rathaus) in the Stuttgart basin, i.e., the MWR at

60 m agl (RT, 305 m asl) and the Windcube at 28 m agl (RD, 275 m asl) (Fig. 2d). Temperature profiles were derived from the MWR measurements every 15 min with a vertical resolution of 50 m up to 250 m above device, increasing towards 200 m at 2000 m above device. The Windcube was operated in the Doppler beam swing (DBS) mode. The three-dimensional wind components were derived from radial wind speed measured at a cone angle of 14.84° at the four azimuth angles of 90, 180, 270 and 360°. The vertical resolution of the wind profiles is 20 m between 40 to 600 m above the device with a temporal resolution of 10 min. The two WLS200 Lidars were operated in a synchronized Range Height Indicator (RHI) scan mode. Vertical profiles of the horizontal wind were retrieved by applying the dual-Doppler Lidar technique at the Feuerwache in the Neckar valley (FW, 222 m asl) (for details see Wittkamp et al., 2021).

The diurnal evolution of the vertical velocity and Lidar-backscatter profiles were measured by KITimkifu at three different locations. Evaluating 300 s statistics allows for the assessment of mixing processes and turbulence. The spatial sampling resolution of the Lidars was chosen to be 18 m (Amt für Umweltschutz, AU and Klärwerk Mühlhausen, KM) and 30 m (Feuerwache Bad Cannstatt, FW), while the temporal sampling rate for all three Lidar systems was set to approximately 1 s.

3.4 Satellite measurements

The satellite-based measurements of the atmospheric composition were obtained by DLRdfd using Sentinel-5P/TROPOMI (TROPOspheric Monitoring Instrument) (Veefkind et al., 2012). TROPOMI was launched by the European Space Agency for the European Union's Copernicus Sentinel-5P mission on October 13, 2017. The satellite follows a near-polar, sun-synchronous low-earth orbit and provides daily global monitoring of the earth's atmosphere. The daily overpass time over Stuttgart is ~ 12:00 UTC. The multispectral imaging spectrometer enables the retrieval of vertical column densities of SO_2, O_3, CH_2O, (tropospheric) NO_2, CO and CH_4 as well as aerosol and cloud parameters. The spatial resolution for the parameters considered in this study at the nadir was $3.5 \times 7.5\,km^2$ and has been improved to $3.5 \times 5.5\,km^2$ on August 6, 2019.

The main objective of 3DO and the IOPs in particular was to obtain and analyze atmospheric physical and chemical parameters using satellite and aircraft-based measurements in order to examine the variability of the urban atmosphere in three dimensions (Erbertseder et al., 2020). In addition to aircraft measurements, satellites provide independent, spatially and vertically integrated observations that are available for any city worldwide. For maximum synergy, the airborne measurements by DLRpa were coordinated with the overpass times of the Sentinel-5P satellite when possible. Specific objectives were the evaluation of the new TROPOMI instrument, with its unprecedented spatial resolution to map the urban pollution island of Stuttgart and to reveal possible urban plumes. Therefore, daily observations of tropospheric NO_2 were evaluated and level 2 data products of version 1.2 were applied (van Geffen et al., 2019). Details on the retrieval, data preparation and discussion of the error budget can be found in Müller et al., 2022 and van Geffen et al., 2022.

4 Results and discussion

The data presented in this paper were collected during an IOP where additional measurements were performed. The following weather conditions were the preconditions for IOP days: autochthonous weather conditions, no rain, wind speed on the ground less than 3 m/s, no fog, no clouds (less than 5/8), maximum air temperature more than 25 °C, formation of a nocturnal surface inversion.

Atmospheric processes or phenomena in and around the urban boundary layer are investigated with this data set. A selection of results, considered to be of particular interest are shown in this section.

4.1 Meteorological conditions in the convective boundary layer

Stationary monitoring stations at different locations in Stuttgart provided the temporal variation of different parameters. Fig. 3a shows climate station observations of air temperature from the stations of SB, LB, NB, MS and SZ with a maximum distance between the stations of 9.7 km. Maximum air temperatures on both days were quite similar, reaching a maximum temperature of about 27 °C on 8 July 2018 and about 28 °C on 9 July 2018. While station air temperatures from mid-morning (09:00 UTC) to early afternoon (16:00 UTC) did not differ more than about 2 K, differential cooling in the evening and during nighttime caused the formation of spatial air temperature differences up to about 5 K. It can be noticed that the onset of cooling in the afternoon started earlier and was more rapid at the stations NB and LB, which are located in well-known cold air source areas for the ventilation of the city center by cold air drainage flows (Schädler and Lohmeyer, 1996). MS and SZ are located within the densely urbanized Stuttgart basin and the air temperature was higher there, during nighttime, due to the urban heat island effect. As evident from the Schnarrenberg station (SB) solar insolation on both days can be characterized being almost undisturbed by clouds up to 11:00 UTC. Later on, convective clouds – Cumulus humilis and mediocris – temporally decrease the downwelling solar flux. While irradiances measured at SB as the site is not affected by shading effects caused by trees or terrain such has to be considered at NB (until 09:30 UTC and around noon) and RS (until 07:15 UTC). Terrain related effects such as reduced solar downwelling flux at near surface level due to shading contribute to the development of temperature gradients between the city center and the suburban

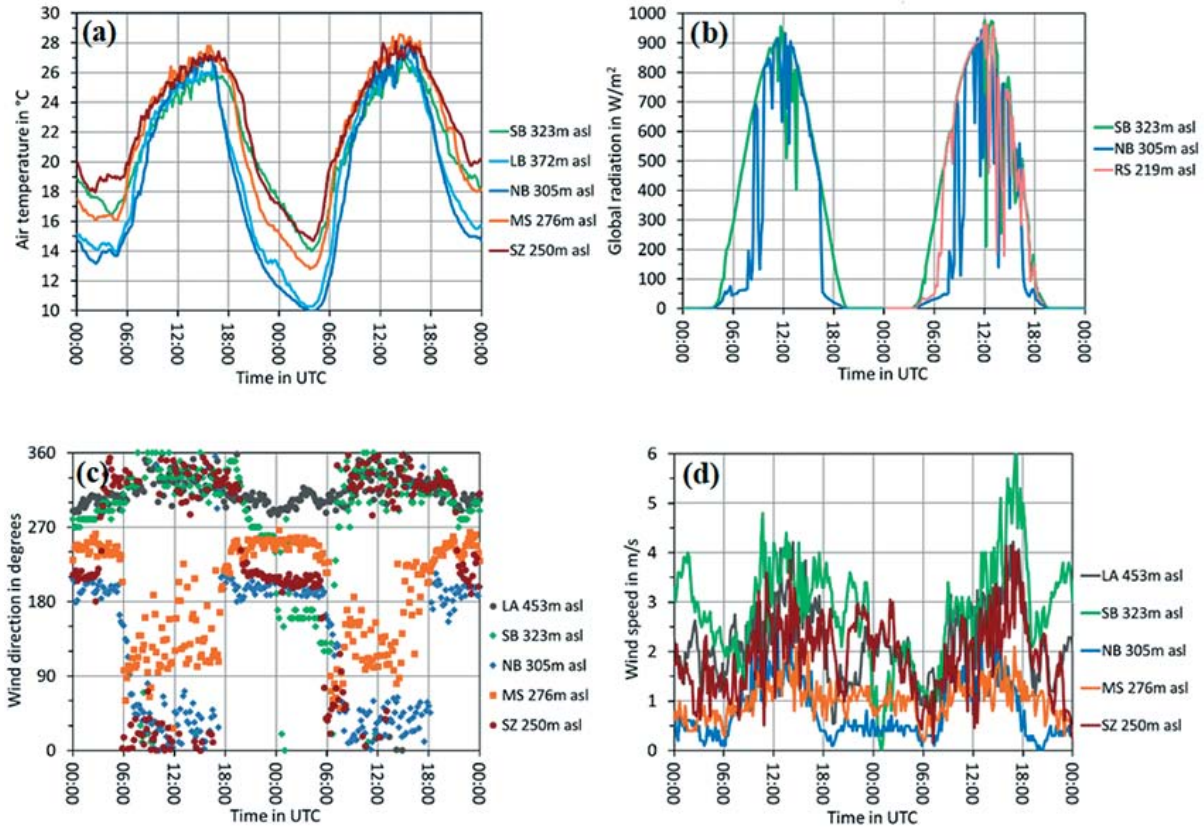

Figure 3: (a) to (d): a) IOP time series of 10-minute mean values of air temperature measured by DWDku1 at the meteorological stations Schnarrenberg (SB), Leonberger Str. (Heidenklinge, LB), Nesenbach valley (Böblinger Str., NB), Möhringer Str. (corner Böheimstr., MS), and Schwabenzentrum (city center, SZ) on 8 and 9 July 2018. SZ air temperature was observed at the top of a 25 m high building, while sensor height at all other stations was 2 m agl. b) Irradiance observations at SB, NB and RS on 8 and 9 July 2018 c) Time series (10-minute mean values) of wind direction and d) wind speed (right) at the climate stations Lauchäcker (LA), Schnarrenberg (SB), Nesenbach valley (Böblinger Str., NB), Möhringer Str. (corner Böheimstr., MS), and Schwabenzentrum (city center, SZ) on 8 and 9 July 2018. The positions of the measurement stations are indicated in Fig. 2a.

Nesenbachtal and therefore influence the onset of local thermal circulations.

The observed diurnal cycles of wind direction and speed at selected climate stations are shown in Fig. 3c and Fig. 3d, respectively. Wind sensor height at these stations was 16 m agl (LA), 10 m agl (SB, NB), and 2 m agl (MS). At SZ, wind and air temperature were observed at the top of a 25 m high building, while sensor height at all other stations was 2 m agl. The LA station is located about 200 m above and about 6.5 km southwest of the Stuttgart city basin. Northwesterly winds prevailed at LA station during day and night, which is in alignment with the direction of the synoptic scale flow during the measurement campaign. The secondary maximum in wind speed at LA after 23:00 UTC coincides with the onset of the low-level jet observed at this height at various vertical sounding sites in Stuttgart. During the daytime, the northwesterly large-scale winds were also observed at the SB hilltop site and SZ city center rooftop site. After sunset, the northwesterly wind at SB is influenced by drainage winds in the Feuerbach valley and gradually veers in westerly directions. After midnight, the depth of the Neckar valley wind reached SB hilltop and the surface wind turned to southerly directions. Nighttime wind observations at stations NB, MS, and SZ show the pronounced development of down-valley winds, known as the Nesenbach valley wind (Figs. 3c and d), which is caused by cold air flow drainage from the cold air production area in the hilly terrain surrounding Stuttgart city center (see Fig. 1b). Following the local alignment of the valley axis, the down-valley winds from the Nesenbach valley show a south-southwesterly (NB, SZ) or a west-southwesterly (MS) direction. Daytime up-valley wind components at these stations are believed to be caused by a combination of channeled large-scale winds and thermally driven valley winds.

Figs. 4a–d show the air temperature results from FZJiek8 and DWDku1 at different times of the day in UTC during the measurement campaign. The sunrise and sunset times on 08.07.2018 were 3:29 UTC and 19:27 UTC, respectively and on 09.07.2018 were 3:30 UTC and 19:27 UTC, respectively.

FZJiek8 measured the air temperature in the city and its surroundings to characterize its spatial distribution on a wider scale. As one measurement drive took more than two hours, the measured temperature was plotted against

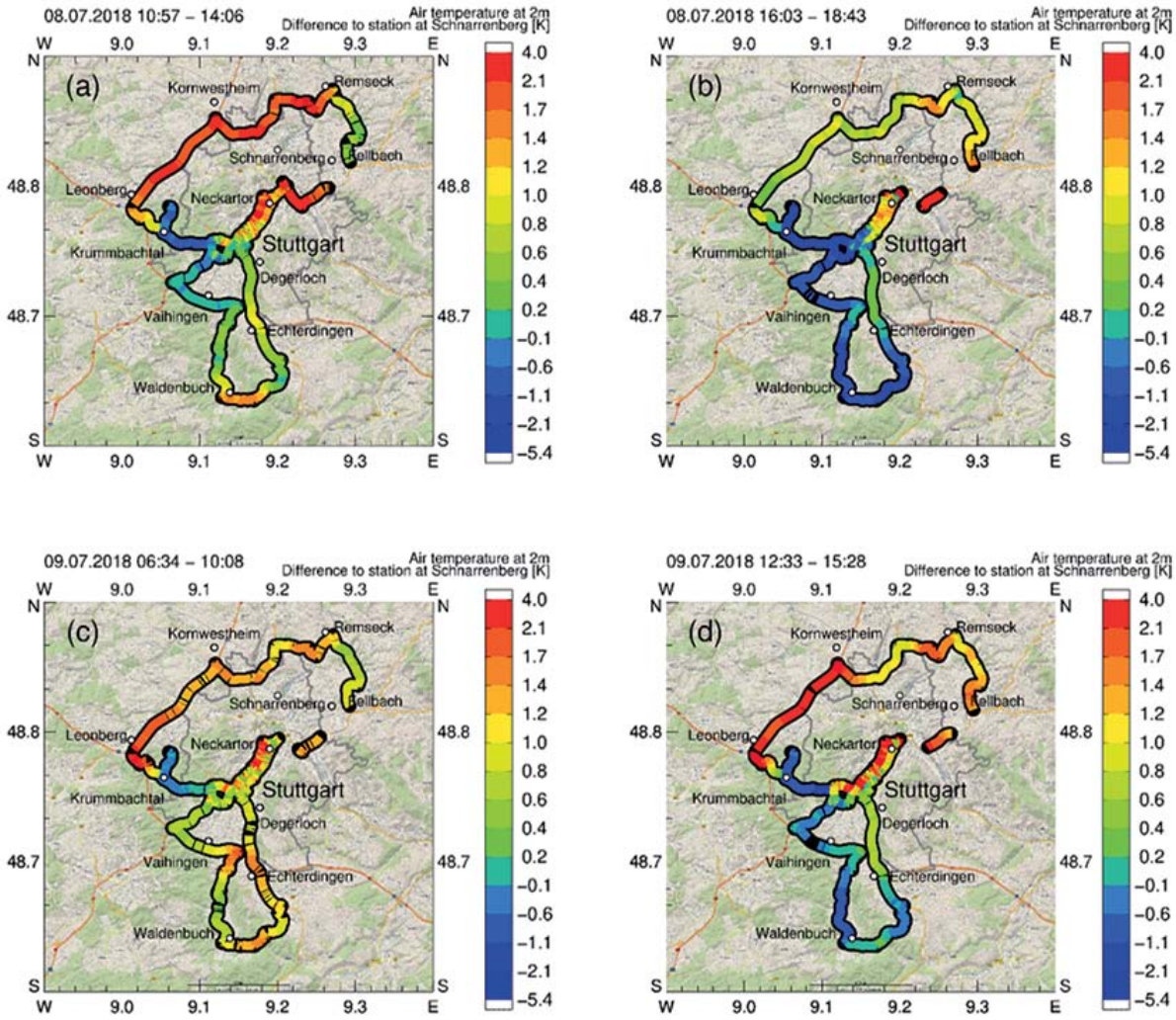

Figure 4: (a) to (d): Temperature difference between mobile measurements by FZJiek8 and DWDku1 in Stuttgart on 8 (4a and 4b) and 9 July (4c and 4d) 2018 and a reference station (SB).

the data of a reference station SB to correct for effects due to the different measurement times. The temperature differences were calculated for each time step by subtracting the values at the reference station from the measured value. As expected, the temperatures in the city were higher than in the surroundings. Unusual and in contradiction to Fig. 3a is, that the temperature gradients were smallest during the morning (Fig. 4c) and largest in the afternoon (Fig. 4b) when the temperature in Krummbachtal was 9 K lower compared to the temperature at Neckartor. During the day temperature in the plain north of Stuttgart, e.g., in Kornwestheim, Leonberg and Remseck reached the same values as at Neckartor in the center of Stuttgart. The two measurement sites considered differ fundamentally in terms of their land use: while the Krummbachtal lies in the middle of a dense deciduous forest, the 6-lane B14 runs through the center of Stuttgart and is additionally bordered on one side by dense development in the area of the Neckartor.

It is well known that the biophysical effects of forests in summer can be responsible for significant temperature differences during the day compared to non-forested areas. (Li et al., 2015) used satellite data analysis to show temperature differences between forested and non-forested terrain: mean ΔLST of up to 6 K. Mobile meteorological measurements by DWDku1's instrumented car moved from the suburb Kaltental along the Nesenbach valley and the tributary Heidenklinge via Stuttgart city center to the Unterer Schlossgarten (see Fig. 2b). Air temperature variations due to terrain height and land cover heterogeneity were strongest during evening and night-time and reached up to about 8 K. Lowest temperatures were observed in the Nesenbach valley in Kaltental and highest temperatures were captured in and around the city center. As expected the Unterer Schlossgarten represents a park cool island (Spronken-Smith and Oke, 1999; Yan et al., 2018). During daytime temperature differences along the transect only reached up to about 4 K due to strong atmospheric mixing.

The formation of thermal winds between the city and the surrounding area is caused by different surface and material properties of urban and rural spaces. An insight into how differently various surfaces heat up during the day is given by a GoPro-IR comparison (Fig. 5a and b)

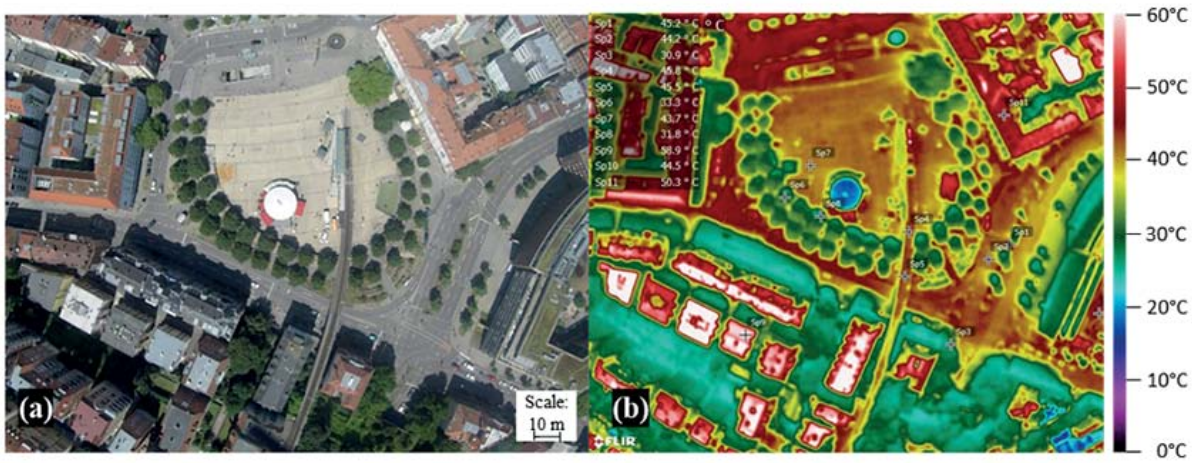

Figure 5: (a) and (b): (a) GoPro image and (b) IR image of 8 July 2018 (10:40 UTC) at Marienplatz Stuttgart measured by LUHimuk.

with a corresponding table of surface temperatures. During the day, almost all surfaces heat up, sometimes to over 40 °C (the emissivity was constantly set at 0.9 for all surface types). Only the fountain area in the north and the treetops remain in the range of around 30 °C (see Fig. 5b). Shaded areas in the inner-city area also remain much colder: For example, a shaded and an unshaded asphalt surface around midday show a temperature difference of 13.3 K. Extensive roof greening also keeps the roof and the adjacent residential or commercial areas up to 5.8 K (compared to pitched roof) or up to 14.4 K (compared to the flat roof without greening) cooler.

Table 2 shows the surface temperature results of different materials at different times. Solid and sealed surfaces such as asphalt, stone slabs or roof surfaces are able to store a huge amount of the incoming solar radiation as heat energy due to their high heat capacity and emits it back to the atmosphere only gradually at night. Vegetated and/or less densely sealed surfaces such as track beds or roadside greenery behave differently. At night, they tend to cool faster, shown in Table 2, e.g. at about 21:40 UTC (comparison of SP1, 4, 5, 6 vs. SP2, 3, 7, 8). As there are predominantly faster-cooling surfaces in the surrounding area, (near-ground) cool winds leading into the city are developing. Roof surfaces play a special role. Although roof surfaces on the one hand cover the largest temperature range in the diurnal cycle and cool down the fastest, they do not play a role in the inner-city cold-air process because they are not connected to the ground but to the occupied buildings with an estimated indoor temperature of 20 °C, thus there is not much contribution from the roofs to the inner-city cold air production because there is permanent energy input from the inner part of the houses into the direction of the roofs.

Vertical turbulence in the boundary layer was studied using the wind Lidar observations at three different locations in and near the city (Fig. 6a–c). Evaluating 300 s statistics (moving averages $\mu(w)$) and corresponding standard deviations $\sigma(w)$ of the vertical velocity, w, which was recorded with roughly 1 Hz data rate, allows for assessment of mixing processes and turbulence. The time scale of 300 s was chosen, so that the largest symmetrical eddies (characteristic velocity >1.5 m/s and length scale >450 m) do not contribute to the turbulence data but to the average velocity data, assuming stationary turbulence. The differences in $\sigma(w)$ indicate stable atmospheric conditions during the night and unstable conditions during the day, when mixing is much stronger (Fig. 6). The mixing sets on shortly after sunrise and decays during the afternoon until about two hours before sunset. An example of a turbulent layer within the nocturnal stable boundary layer is shown in Fig. 6a. During the time between 01:30 UTC and sunrise, a layer around 300 m above the instrument can be identified, in which $\mu(w)$ shows multiple inflections in the profile, while clouds are present around 2.000 m above the instrument. After sunrise, around 05:00 UTC the clouds cleared and the aforementioned layer is resolved by turbulent mixing with increases in $\sigma(w)$. The increase in global irradiance measured at the surface (Fig. 6a) is accompanied by the growth of the thermally forced boundary-layer reached up to 400 m at 07:00 UTC, 750 m at 08:00 UTC, 900 m at 09:00 UTC and 1.400 m at 09:30 UTC.

During nighttime, the stations in the urbanized surroundings (AU and FW) showed more residual vertical motion, $\sigma(w)$ was higher at night below 500 m in Figs. 6a and Fig. 6c compared to Fig. 6b. During the daytime, the magnitude and duration of structures in w show differences between the sites during the campaign day. In Neckar valley, the vertical velocity maxima extended deep into the boundary layer (see Fig. 6c, 13:00 UTC) with an observed duration of roughly 10 minutes. In the urban valley (see Fig. 6a, 13:15 UTC) a longer lifetime with a local maximum of w located around 500 m above the surface can be seen. The outskirts showed lower values in average vertical motion and shorter durations of these large structures. Persistent low-level flow modification in the urban valley during summer was reported

Table 2: Surface temperatures results of different materials at different times of the day at Marienplatz, Stuttgart Sunset time (July 8): 19:27 UTC; Sunrise time (July 09): 03:30 UTC.

Nr.	Material/Object	July 8 and 9, 2018 (Time in UTC)					
		10:40	18:40	19:40	21:40	02:40	04:40
		Surface temperature in °C					
Sp1	Roadside greenery	45.2	25.8	24.3	17.6	12.7	18.0
Sp2	Asphalt (unshaded)	44.2	31.0	30.1	22.9	17.2	20.5
Sp3	Asphalt (shaded during daytime)	30.9	26.3	25.4	18.5	15.8	19.1
Sp4	Trackbed (unshaded)	45.8	29.6	28.0	18.7	12.9	16.8
Sp5	Trackbed (shaded during daytime)	45.5	28.0	26.6	18.1	12.4	16.1
Sp6	Tree crown	33.3	24.9	23.6	16.6	12.0	19.3
Sp7	Marienplatz (unshaded)	43.7	30.4	30.0	22.3	16.4	20.7
Sp8	Marienplatz (shaded during daytime)	31.8	27.0	26.2	21.2	16.5	20.8
Sp9	Flat roof (unshaded)	58.9	21.5	19.0	12.0	8.5	13.9
Sp10	Flat roof (extensive roof greening, unshaded)	44.5	23.0	21.9	14.5	9.9	15.9
Sp11	Peaked roof (unshaded)	50.3	23.6	23.9	15.1	10.1	16.0

by Zeeman et al. (2022). The combined effect of differences in thermal forcing (e.g., surface modification) as well as obstruction through topography (and thus movement speed of structures) need to be considered when interpreting the data presented here.

In Fig. 6 clouds can be seen in the aerosol backscatter data during the night between 02:00 UTC and 05:00 UTC around noon between 11:00 UTC and 14:00 UTC for all three locations (refer to Fig. 2d). The plume seen in Fig. 6b during night between 02:30 UTC and 06:30 UTC has been attributed to the exhaust chimney of the biomass combustion processing unit at the sewage plant. The plume has been detected on multiple occasions throughout the campaign.

In the afternoon, the base of the elevated temperature inversion detected by radiosonde ascents reached heights of about 2.350 m asl on 8 July 2018 and up to about 2.700 m asl on 9 July 2018 (Figs. 7a and b). This indicates for both days the development of deep afternoon mixed layers favoring strong vertical mixing. During the night from 8 July 2018 to 9 July 2018 radiosonde ascents show the development of a deep cold air layer reaching up to about 900 m asl.

While radiosoundings from the SB hilltop near the Neckar valley show a rather simple vertical structure of the cold air layer, the soundings from SP (southwest of the city center) reveal a complex multi-layered structure of the nocturnal temperature stratification. The SP soundings at 19:00 UTC, 23:00 UTC, and 03:00 UTC show the presence of a ground-based, approximately 50 m deep layer with characteristics of a nocturnal mixed layer, possibly generated by a combination of thermal mixing (release of heat stored in buildings during daytime) and mechanical mixing due to Nesenbach valley drainage flow from southwesterly to westerly directions. This shallow mixed layer is capped by a sharp temperature increase of about 2 K at 19:00 UTC and about 5 K at 23:00 UTC and 03:00 UTC (Fig. 7a). This low-level inversion represents an important barrier to the vertical dispersion of air pollutants emitted near the surface (e.g. traffic emissions). Between the inversion above the mixed layer and the residual layer aloft, the radiosoundings show the presence of an approximately isothermal layer reaching up to about 500 m asl at 19:00 UTC and 23:00 UTC and up to about 900 m asl at 03:00 UTC.

The synopsis of data from multiple vertical sounding sites and surface stations at selected times provides insight into spatial variations in stratification, local wind characteristics, and thermal forcing of local winds, Fig. 7c–e jointly depicts observations of potential temperature and wind at various sites from the Kaltental suburb in the southwest to the Neckar basin in the northeast on 8 July 2018 at 23:00 UTC. The vertical soundings of potential temperature show that the strong inversion capping the shallow nocturnal mixed layer varies around 70 m between SP and MP, i.e. the inversion is tilted from the suburb in the southwest towards the city center, approximately following the height of the underlying terrain. The profiles at the vegetated SG near the Neckar basin and at the hilltop site SB do not show a shallow mixed layer at the lowest levels.

Temperature observations at the surface stations LA, (453 m asl), LB (372 m asl) and NB (305 m asl), located in the nocturnal cold air drainage catchments of the Nesenbach valley show considerably lower values than measured at the same elevation by vertical soundings in the Stuttgart basin and the Neckar basin. The temperature deficit at LA is about 5 K and 8 K at 16 m and 2 m agl, respectively. At LB and NB stations the temperature deficits at 2 m agl range between about 2 K relative to the SP sounding and 7 K relative to the SG sounding. These temperature deficits reveal a strong forcing of drainage winds early in the night (23:00 UTC).

Wind measurements below 400 m asl show southerly to westerly wind directions indicating the presence of drainage winds which are decoupled from large scale northerly winds aloft (Fig. 7d). Vertical soundings of wind speeds at valley sites MP and SG show level wind maxima in the lowest 100 m agl similar to textbook illustrations of nocturnal mountain winds. The SODAR

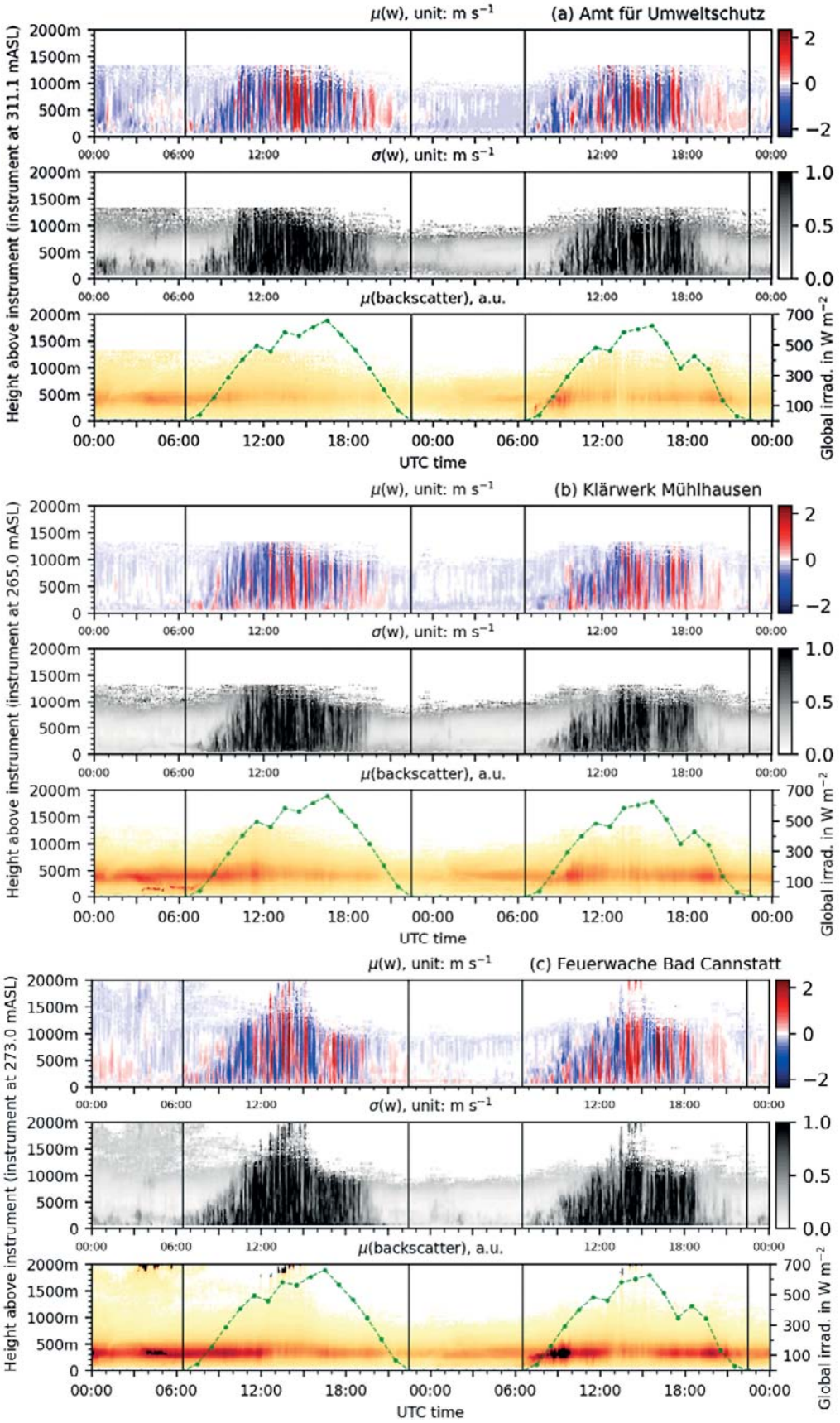

Figure 6: (a) to (c): Doppler Lidar measurements in Stuttgart showing 300 second averages μ (colored) and standard deviations σ (greyscale; middle two panels) of vertical velocity w (averages in upper two panels) and Lidar-backscatter profiles (averages in lower two panels) for 08–09 July 2018 measured by KITimkifu. Vertical lines indicate astronomical sunrise and sunset, while the green curve shows global irradiation as measured hourly at KM (lower panels). The positions of the measurement stations are indicated in Fig. 2d. The vertical coordinate here is height above surface in meters, where the roof height for rooftop measurements is not part of the surface height.

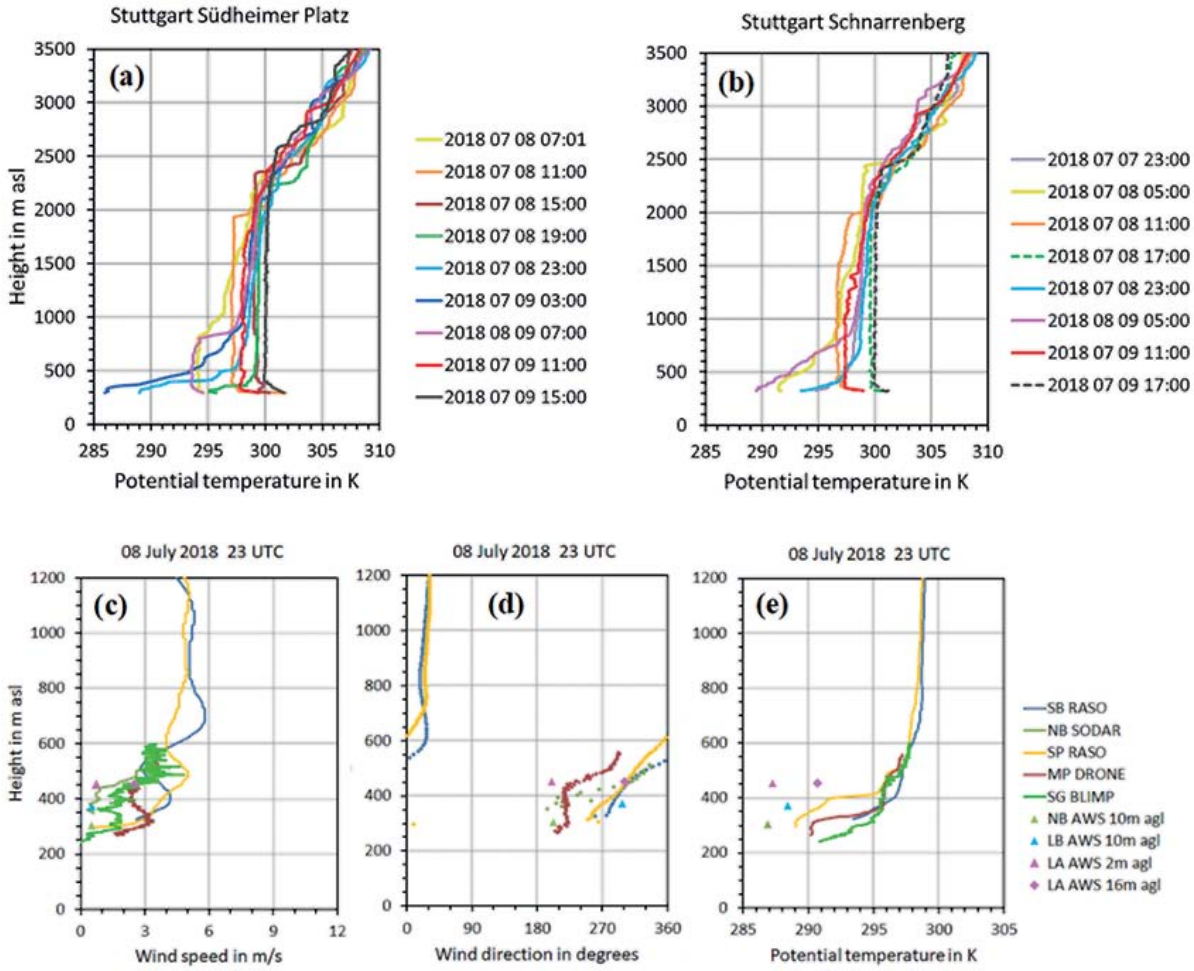

Figure 7: (a) to (e): Temporal evolution of vertical air temperature profiles at a) Südheimer Platz (SP) and b) Schnarrenberg (SB), Stuttgart measured by DWDku1 on 8 and 9 July 2018. Vertical profiles and surface station observations of c) wind speed, d) wind direction, e) potential temperature on 8 July 2018 at 23 UTC. SG = Schlossgarten, SB = Schnarrenberg, NB = Nesenbach valley, SP = Südheimer Platz, MP = Marienplatz, LB = Leonberger Str., LA = Lauchäcker. The positions of the measurement stations are indicated in Fig. 2.

system at the NB site, with its lowest range gate at 45 m agl, did not capture a low-level wind maximum. The radiosonde sounding at SP shows strong wind shear near the surface with wind speeds reaching about 3 m/s at 30 m agl. Further up, wind speed keeps increasing with height, reaching a wind speed maximum of about 5 m/s above ridge height (500 m agl).

The temporal development of stratification in the atmospheric boundary layer from 04:00 UTC at 8 July 2018 to 9 July 2018 on 19:00 UTC is shown in Fig. 8a. During both nights, a surface inversion developed. However, as clouds prevailed on the first night (Fig. 6), at 05:00 UTC on 8 July 2018 the inversion strength was only about 0.6 K/100 m, while on the second night, which was cloudless, the inversion was much more pronounced. For example, at 05:00 UTC on 9 July 2018, the temperature gradient in the layer below 700 m above the device reached about 1.2 K/100 m. Well-mixed convective boundary-layers started to form between 08:00 UTC and 09:00 UTC, as also visible in the radiosounding observations (Fig. 7).

The temporal evolutions of horizontal wind speed in the Stuttgart basin (RD) and the Neckar valley (FW) are presented in Fig. 8b and c. During the night from 8 to 9 July 2018, between 23:00 UTC and 05:00 UTC a low-level jet (LLJ) was detected at both sites centered around 500 to 550 m asl with maximum wind speeds of 5 m/s from northwesterly direction. The presence of LLJs above the mean ridge height of the surrounding hills of Stuttgart and the Neckar valley (470 m asl) was already described by Wittkamp (Wittkamp et al., 2021; Kiseleva et al., 2022). In the Neckar valley (FW), a southwesterly wind below the LLJ was established on the corresponding night from 8 to 9 July 2018, approximately 3 m/s in strength (Fig. 8c). That means a thermally-driven down-valley wind developed in the Neckar valley. In the Stuttgart basin, in accordance with the orientation of the basin, a weak thermally-driven southwesterly wind of around 1.5 m/s was observed (Fig. 8b). In the morning after around 8:00 UTC on both 8 and 9 July 2018, with increasing insolation, a convective boundary layer developed and the horizontal wind from northerly

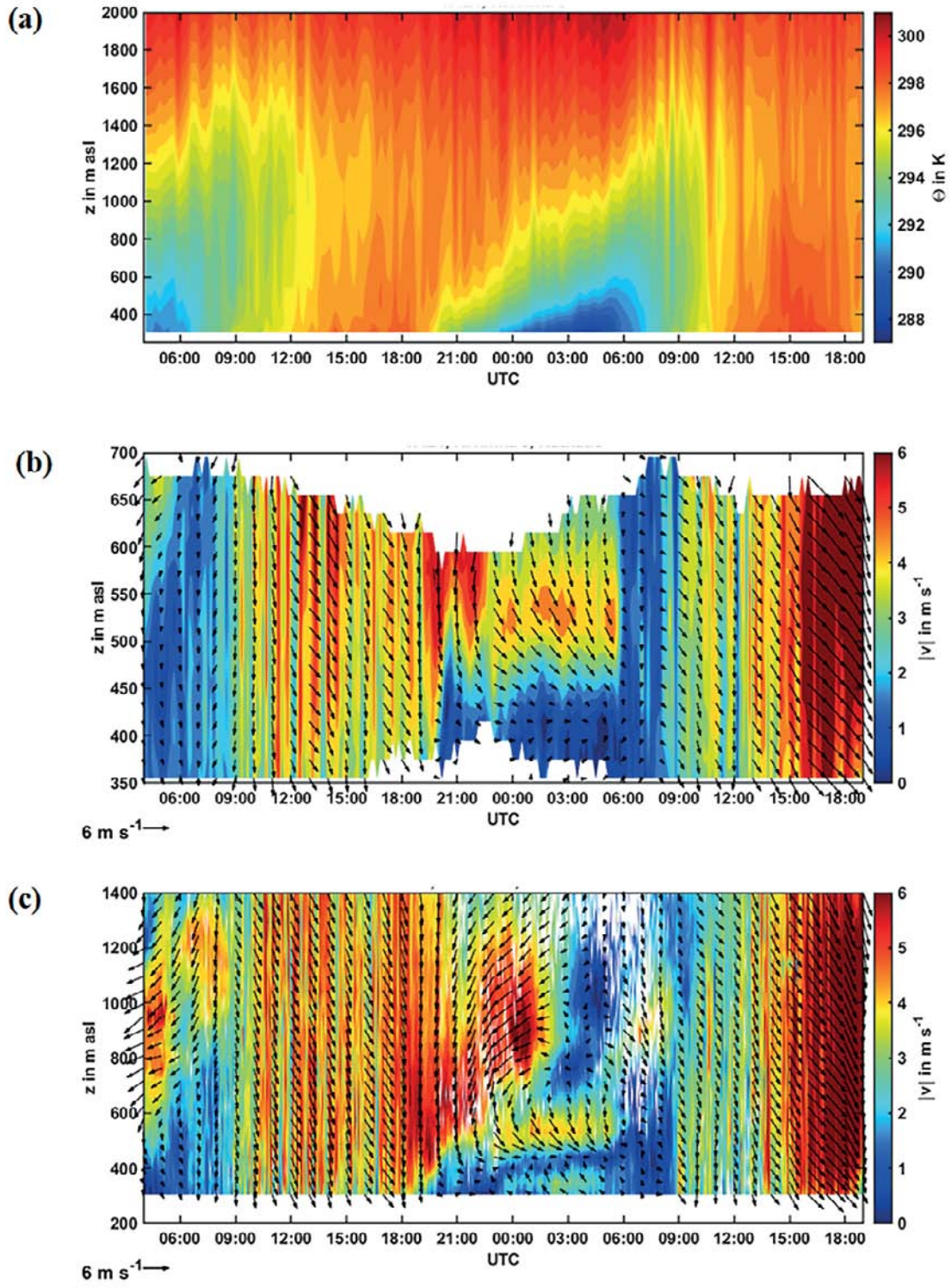

Figure 8: (a) to (c): Time-height cross sections (a) of the potential temperature (color coded) from microwave radiometer measurements at RT in the Stuttgart basin and (b) of the horizontal wind speed (wind vectors) and absolute value of the horizontal wind speed (color coded) based on Windcube measurements at RD (c) and virtual-tower technique at FW in the Neckar valley on July 8 and 9, 2018 measured by KITimktro. The wind vectors are 1-hourly averages with northerly winds pointing downwards and westerly winds to pointing to the right. The positions of the measurement stations are indicated in Fig. 2d.

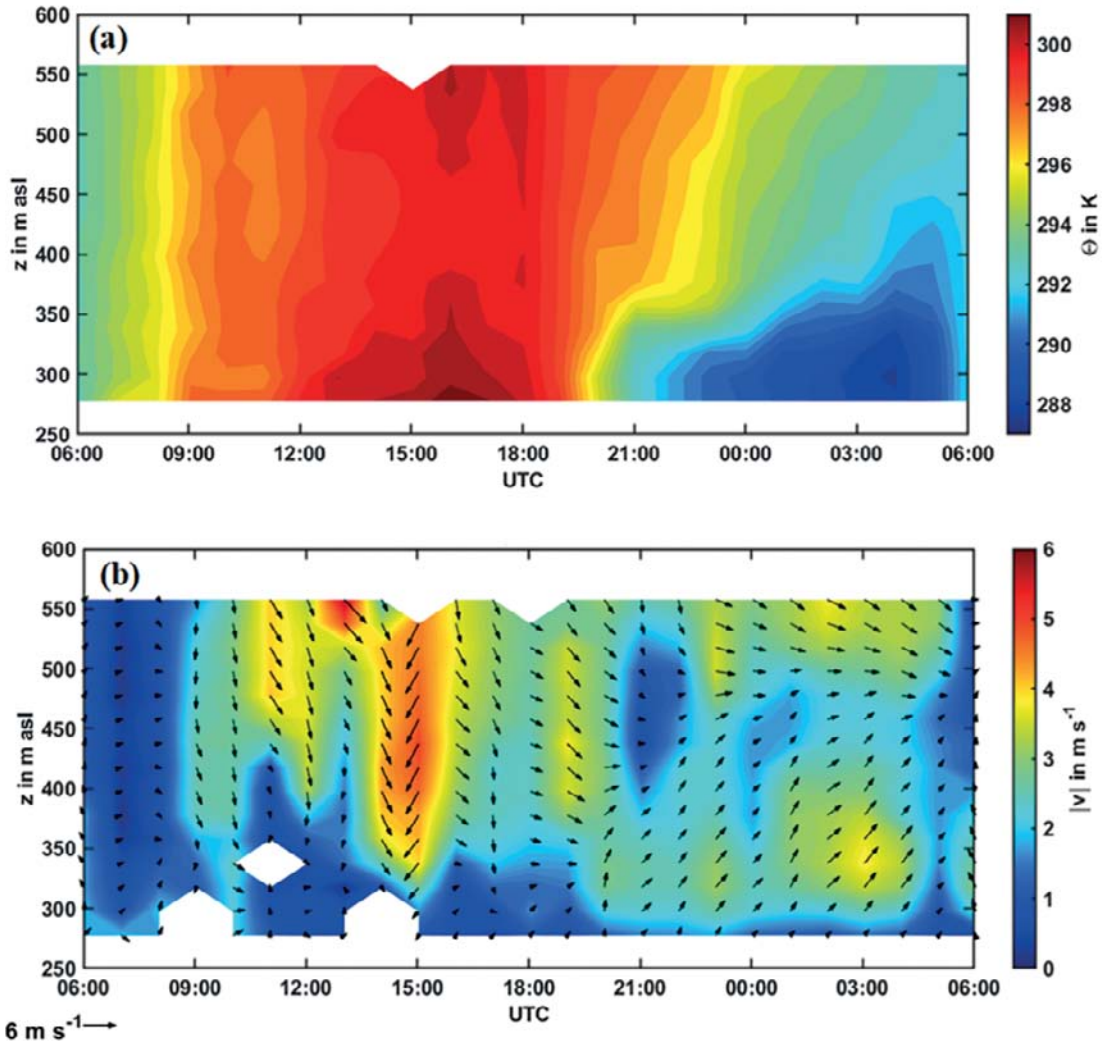

Figure 9: (a) and (b): a) Time-height cross-section of potential temperature at MP Stuttgart measured by LUHimuk (July 8 and 9, 2018) b) Time-height cross-section of wind speed and wind direction at Marienplatz Stuttgart measured by LUHimuk (8 and 9 July 2018).

to northwesterly direction prevailed at all heights, i.e. momentum was vertically well mixed due to turbulence, ranging around 4 to 5 m/s on the first and about 5 to 6 m/s on the second day.

Regarding daytime maxima, the (ground-level) air temperature has a time lag of about 2 to 3 hours compared to the surface temperature. Fig. 9a shows the contour plot of the potential temperature measured with a radiosonde installed at a drone, which shows that the highest temperatures (301.3 K) were reached not until around 16:00 UTC. At sunset, the predominant neutral stratification bit by bit transformed into a stable stratification, shown by a developing inversion layer. For the first time that day, at around 20:00 UTC the ascent was exposed to an increasing of temperature with height. It can be observed that the inversion layer never started directly on the ground during the measurements, indicating the still not completely cooled-down urban surfaces. In some hours of the second half of the night, the vertical thickness of the inversion cannot be completely resolved in spite of measurements up to almost 300 m agl. At sunrise, the inversion then collapsed from bottom to top. During the last ascent around 06:00 UTC in the morning on 9 July 2018, a slightly elevated inversion with a temperature gradient of 1 K was still measurable.

Hexacopter observations show low wind speeds up to a maximum of 6 m/s on the first day of the measurement campaign (Fig. 9b), similar to the isopleth diagrams (Fig. 8b). The maximum wind speed was recorded during daytime (13:00 UTC on 8 July 2018 at a height of about 550 m asl), while the lowest wind speeds were determined at night, which can be explained by subsiding convection and turbulence processes. The wind direction was predominantly from the south during the first three hours of the measurements, turned to the north as the day progressed, then turned to westerly directions in the evening and night. However, near the ground there was a southwesterly wind current at night. This ground-level air flow might partially be thermally induced and represents a balancing wind system between the warmer city center (MP) and the cooler and more rural NB, respectively the penetrating drainage wind.

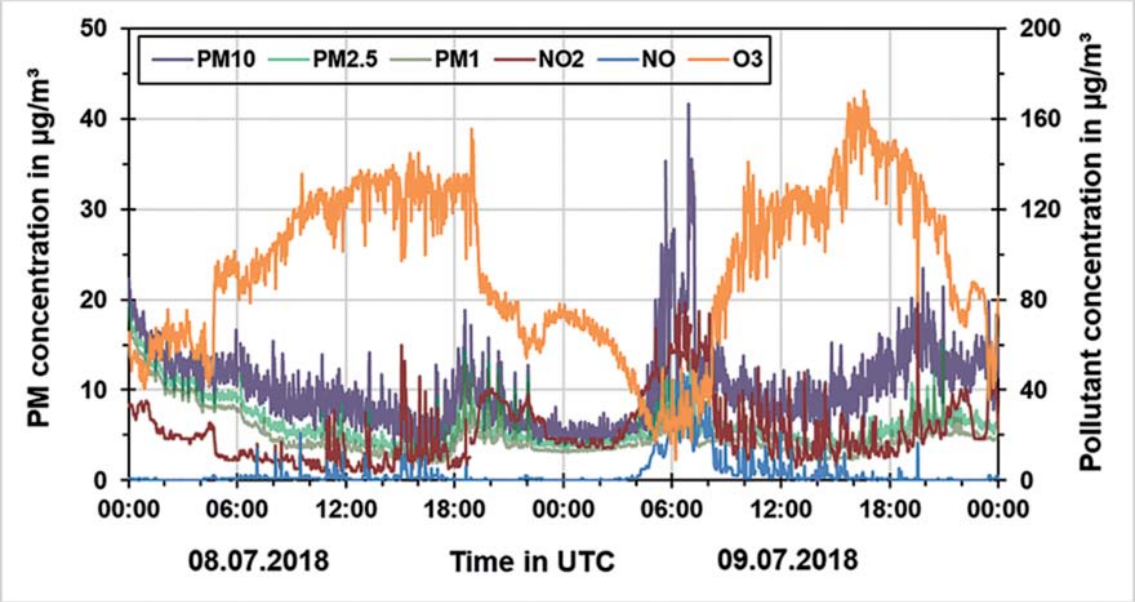

Figure 10: Time series (1-minute mean values) of air pollutant concentrations measured by USifk at Marienplatz (MP) Stuttgart on 8 and 9 July 2018. The positions of the measurement stations are indicated in Fig. 2a.

4.2 Urban air pollution situation in Stuttgart

The air quality measurements at the stationary monitoring station MP Stuttgart provided an overview of the ambient air pollutant concentration near the city center of Stuttgart, shown in Fig. 10. Since 8 July 2018 was a Sunday, it can be seen that the PM10 concentration during the day was low and varied between 5 and 20 µg/m^3. Higher PM10 concentrations were observed on 9 July 2018 (Monday) from 05:00 to 07:00 UTC because of the morning rush hour. The PM10 concentration decreased until noon and increased again after 16:00 UTC and reached a second maximum of around 20 µg/m^3 at 19:00 UTC. The evening PM peak is caused by the rush hour emissions, but at the same time the urban boundary layer becomes more stable and the formation of the nocturnal temperature inversions starts. PM2.5 and PM1 concentration during the whole time was mostly below 10 µg/m^3. The gaseous components NO and NO_2 behaved in the same way as PM. The peak NO and NO_2 concentrations during the morning rush hour reached about 40 and 80 µg/m^3, respectively. The O_3 concentration during the whole measurement campaign was in the range of 100 to 160 µg/m^3 during the daytime for both campaign days. It reached a concentration of below 80 µg/m^3 in the nighttime. The stagnant meteorological conditions led to the formation of a shallow nocturnal boundary layer after sunset at 19:30 UTC and a subsequent increase in nitrogen oxides and particles. At the same time, the ozone concentration was reduced by the reaction with NO. The nocturnal boundary layer is first resolved (4:00 to 7:00 UTC) and then totally dissolved (after 7:00 UTC), then typically ozone from the overlying residual layer is mixed down to the ground, increasing the ozone concentration there despite the simultaneous increase in nitrogen oxide emissions due to increasing traffic. The onset of photolysis shifted the photo-stationary equilibrium from NO_2 to ozone and NO, which also contributed to the increase in ozone concentration. Compared to these processes, local ozone production was of little importance. Detailed result analysis of these measurements is done by USifk (see Samad and Vogt, 2020).

Fig. 11 shows the urban boundary layer of Stuttgart as sampled by DLRpa from the DLR Cessna aircraft and FZJiek8 with MobiLab on 9 July 2018. In Fig. 11a, the vertical CO_2 distribution is described, which is a proxy for the distribution of nitrogen oxides. The panels show observations above the city of Stuttgart along the southeastern side of the Cessna flight box and corresponding mobile ground-based observations during the morning and afternoon flights. The background shading displays a vertical interpolation of the observations using the Kriging algorithm (e.g. Fiehn et al., 2020). Due to the nature of airborne in-situ observations, this kind of interpolation between point measurements along the flight track will only allow for a qualitative impression of the distribution. Nevertheless, it shows the temporal evolution of the boundary layer and the resulting distribution of emissions. The city center stretches roughly from the Marienplatz to the Feuerwache near the river Neckar. Using vertical profiles of water vapor mixing ratios and potential temperature, the mixed layer height for the morning flight is estimated to be 930 m asl. Trace gas (CH_4) emission from the city accumulated below this altitude, as shown in Fig. 11c. High CO_2 levels prevailed throughout the city center and to a lesser extent north of the Neckar (Feuerwache to Kappelbergtunnel). Southwest of the city center the track was not in the Stuttgart basin and trace gas concentrations were generally lower than within the basin.

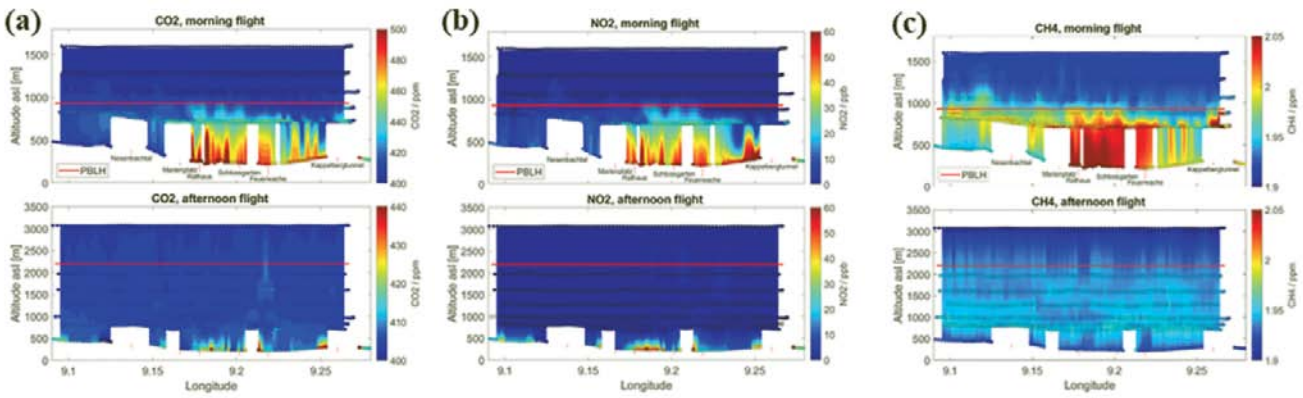

Figure 11: (a) to (c): Aircraft and ground-based mobile in situ measurements on 9 July 2018. Morning flight: 07:30 to 09:40 UTC and 11:15 to 13:45 UTC. Circles show observed values and the background colour their interpolated values. The red line denotes the boundary layer height.

In the afternoon the boundary layer had increased to 2200 m asl and was well-mixed. The trace gas concentrations in all flight levels were similar and only close to the ground enhancements of CO_2 and NO_2 concentrations indicated strong emission hot spots along the highly-trafficked federal highway B14 in Stuttgart. These observations can be used to validate high resolution atmospheric chemistry models in the horizontal and vertical as well as over the time of the flights.

At SG in Stuttgart vertical profiling was performed with the help of a tethered balloon system. The maximum potential temperature in the day was as high as around 303 K and it decreased in the night to 287 K (Fig. 12a). The increase in temperature after sunrise on 8 July 2018 is evident by the layers of higher temperature along the time axis. A stable boundary layer can be seen from midnight to the morning of 9 July 2018 due to a positive gradient of potential temperature, which indicates the presence of a strong temperature inversion. The inversion layer at the surface started to build up on the evening of 8 July 2018 after 17:00 UTC and reached a height of about 350 m above sea level before 5:00 UTC on the morning of 9 July 2018. After sunrise, the stable boundary layer dissolved and a mixed layer was formed as seen by a constant gradient of potential temperature.

The temperature inversion influenced the pollutant concentration as they are confined in the inversion layer. To illustrate, the concentration of PM10 is shown in Fig. 12b. During the first 12 hours (09:00 UTC until 21:00 UTC) of the measurement campaign, PM10 concentrations of around 20 to 30 µg/m^3 were observed close to the ground and the PM10 concentrations were below 20 µg/m^3 at higher altitudes (neglecting the occasional increase in PM10 concentration). As the temperature inversion evolved, the pollutant concentration started increasing in the inversion layer. The PM10 concentration reached between 30 to 40 µg/m^3 at a height of around 400 m asl at around 04:00 UTC. The highest PM10 concentrations were observed in the morning time from 06:00 UTC to 08:00 UTC caused by the morning traffic. This increase in PM10 concentration at the ground affected the PM10 concentration to a height above 500 m asl due to well mixed convective situation. Later on, from 09:00 UTC until 18:00 UTC on 9 July 2018, the PM10 concentration was reduced and fluctuated between 10 to 30 µg/m^3.

By oversampling and averaging all overpasses over a period of time, Sentinel-5P/TROPOMI is able to delineate urban pollution islands as regional or national hot spots in tropospheric NO_2 (Müller et al., 2022). Tropospheric NO_2 is a suitable short-lived tracer for mainly anthropogenic emissions and activity (Erbertseder et al., 2015; Voigt et al., 2022), except for lightning (Perez-Invernon et al., 2022). Fig. 13 (left panel) illustrates the monthly mean tropospheric NO_2 distribution over Stuttgart for July 2018 calculated from 31 overpasses at $0.01° \times 0.01°$spatial resolution. The urban pollution island of Stuttgart is depicted with maximum values of 6.0 10^{-5} mol/m^2 in the city center. Despite the unprecedented spatial resolution of TROPOMI only urban background conditions can be represented. It was further shown in the [UC]^2 project that TROPOMI allows for the detection of urban plumes with the instrument being capable of resolving pollution in the urban boundary layer, Fig. 13 (right panel). The tropospheric NO_2 distribution over Stuttgart from 9 July 2018 at an overpass time of 11:58 UTC confirms the findings of Berlin (Erbertseder et al., 2020) and Paris (Lorente et al., 2019) that urban plumes can be resolved, but to a much smaller extent in this case. There is an indication of a plume in the southeast of Stuttgart, where wind from northwesterly directions transported urban air masses to the surrounding area. The maximum of the NO_2 pollution was transported ~25–30 km downwind (5.5×10^{-5} mol/m^2) up to Kirchheim Teck. The MODIS observations, however, show a band of convective clouds from north to south and prove that the urban area of Stuttgart was partly covered by clouds, which may obscure a possible

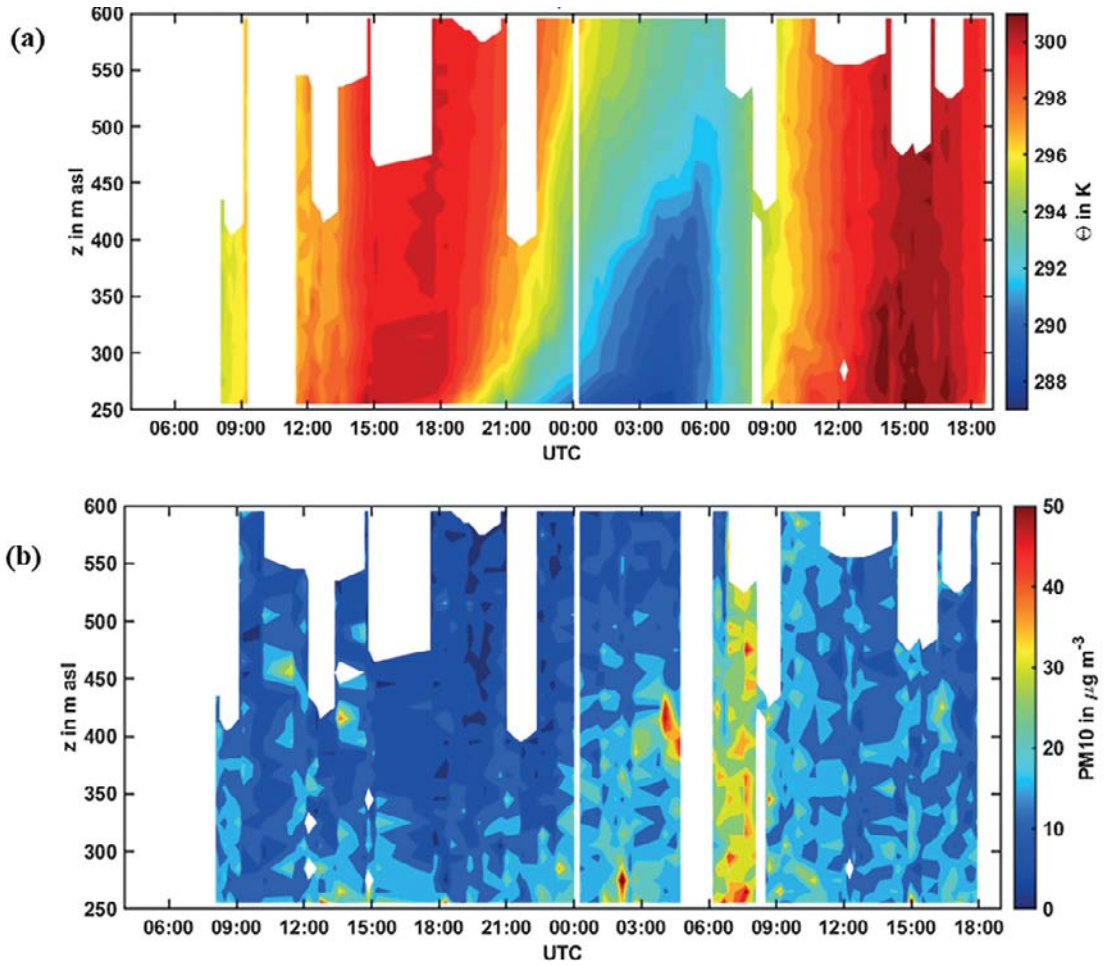

Figure 12: (a) and (b): Time-height cross-section of (a) potential temperature and (b) PM10 at SG Stuttgart measured by USifk (8 and 9 July 2018).

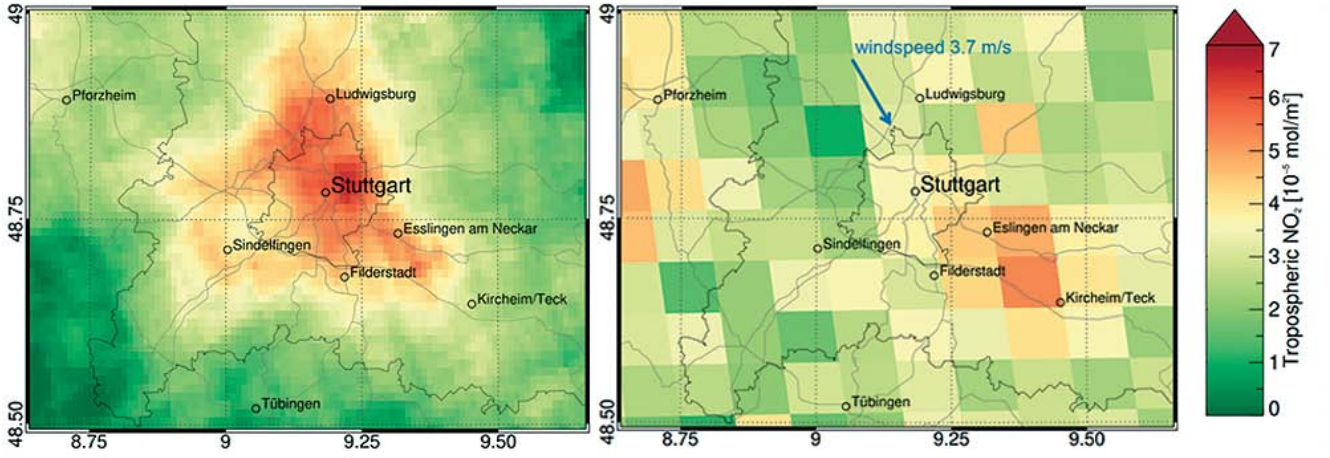

Figure 13: Monthly tropospheric NO_2 distribution over Stuttgart for July 2018 as observed by TROPOMI (left panel). Synoptic tropospheric NO_2 observation on 9th July 2018 at the overpass time 11:58 UTC. An urban NO_2 plume is indicated downwind of the city in the southeast. The corresponding image from Aqua/MODIS shows a band of convective clouds over Stuttgart from north to south accompanied by scattered cumuli throughout the region that might obscure NO_2 in the urban boundary layer.

NO_2 burden. Therefore, the NO_2 observations should be interpreted cautiously. The vertical mixing in the boundary layer and the horizontal dispersion processes demand a more detailed model-based examination which is out of the scope of this paper. The purpose was to demonstrate that these kind of observations offer an additional data source for the evaluation of city-wide trace gas distributions, the closing of mass balances, as well as the examination of coupling urban scale with mesoscale meteorology (especially regarding the wind direction and wind speed).

5 Data preparation and availability

The observational data collected during the measurement campaign on 8 and 9 July 2018 in Stuttgart were converted into the 'Urban Climate under Change' ($[UC]^2$) data standard (Scherer et al., 2019a). The data standard comprises of a self-describing netCDF format (www.unidata.ucar.edu/software/netcdf) which is used worldwide, and a large number of open, free interfaces and applications exist that handle netCDF. A wide variety of data and metadata can be stored in netCDF files. The $[UC]^2$ data standard follows the netCDF Climate and Forecast (CF) Metadata Conventions version 1.7 (cfconventions.org/Data/cf-conventions/cf-conventions-1.7/cf-conventions.html). The mandatory metric coordinate system of the $[UC]^2$ data standard is the *Universal Mercator System* (UTM). Eastings and northings are specified according to the reference system ETRS89 with the GRS80 ellipsoid. The UTM zone 32 referring to the central meridian of 9 degrees (EPSG projection 25832) was applied to all measurement data within the 3DO project including the measurement data of the field campaign in Stuttgart.

The observational data sets described above have been sampled and processed among others as a reference for evaluating the capabilities of the PALM-4U model (Maronga et al., 2019). The preparation of the data for model evaluation included the introduction of a joint data format, the upload of the observational data into a joint database and the employment of a model extension to store additional outputs for the observation sites for all time steps of model integration. All observational data of the field campaign were uploaded to the Data Management System (DMS) operated by the Chair of Climatology at the Technical University of Berlin and can be accessed via the internet (https://dms.klima.tu-berlin.de). All model and measurement data of the entire research campaign $[UC]^2$, not only the data set described in this paper, are open access data and can be accessed through the DMS platform. In the future, another data portal respectively different portals will be installed to provide all data for a long-term period as open access. Detail planning is going on, but not yet finalized.

6 Conclusions

Numerous atmospheric processes in an urban area regarding boundary layer evolution, inversion, local wind systems, urban heat island, etc. were observed with diverse measurement techniques during the described measurement campaign, which can also be taken as a test case to validate the urban climate model PALM-4U.

The obtained data also improves the understanding of the local meteorological and air quality situation of Stuttgart city and its surroundings due to its complex terrain. The urban heat island effect was evident from the results of stationary and mobile air temperature measurements as the higher air temperature was always measured in the Stuttgart basin compared to its surroundings. Relatively lower air temperatures were observed in the lee side (south) of the city in comparison to the windward side (north). Local wind effects caused by the topography were found to determine the concentration of pollutants. Lower wind speeds were observed during the nighttime and the main wind direction in the Stuttgart valley was measured to be southwest, which carried cold air from the hillsides into the city and pollutants to the leeward side of the city into the Neckar valley. The low wind speed favored the accumulation of pollutants in a shallow nocturnal boundary layer close to the surface. During the day, the overall pollutant concentration was reduced by vertical convective mixing.

In the study of different surface types in an autochthonous weather situation, their different heat storage capacities and the associated heating during the day were highlighted. It was found that the highest surface temperatures were measured on highly sealed surfaces on both campaign days, while unsealed or shaded areas showed low surface temperatures. After sunset, the surfaces began to release the energy stored during the day back into the environment as heat and in this way also influenced the near-ground air temperature. Thus, the location Marienplatz in Stuttgart also showed itself as an urban heat spot at night, with heat escaping from the surfaces towards the atmosphere until early morning.

The effect of temperature inversion on pollutant concentrations in the city was investigated. This effect was seen from the results as the pollutants get trapped in the inversion layer and the pollutant concentrations measured during this time increased. Another interesting relationship was observed between the variation of altitude and pollutants i.e. the concentration of the pollutants was relatively higher at the ground as compared to the upper region. This highlights the importance of local emissions for concentrations near the surface and demonstrates the need for accurate emission data and detailed chemical process representation in urban air quality modeling.

The vertical profile measurements have shown that the applied techniques provided a good overview to understand the vertical characteristics of meteorological parameters and pollutants as well as the stability of the atmosphere and extent of the urban boundary layer. It also showed the extent of atmospheric mixing determines the dispersion, dilution and mixing of emitted pollutants. Geographical characteristics of the area affect the meteorological parameters such as wind speed and wind direction which in turn have an impact on

the pollutants and hence the quality of air. In general, higher wind speeds quickly dispersed the pollutants and thus lowered the aerosol concentration. During the campaign, there was enough solar radiation during the day and hence enough convection which resulted in a deep boundary layer and considerable vertical mixing of air masses.

If the vertical mixing is sufficient, increases in boundary layer depth cause a reduction in pollutant concentration near the surface, even though the pollutant emission is constant. This volume effect is dependent on the mixing and dispersion and thus can be impaired by obstacles like buildings or trees. During the night, the temperature and the wind speed were lower which led to a shallow boundary layer and reduced the vertical mixing. The volume in which the pollutants are dispersed is reduced leading to an increase in their concentration. It was found that the air masses near the ground were more polluted with particles and nitrogen oxides than the air masses at higher altitudes as these pollutants are emitted from the ground. In higher altitudes no vertical gradient was observed during the day.

Satellite-based observations from Sentinel-5P/TROPOMI have shown their potential for mapping urban pollution islands and urban pollution plumes even in cities with a complex terrain like Stuttgart. The new sensor constitutes an addition to traditional measurement setups for mapping city-wide and mesoscale trace gas distributions, the closing of mass balances, as well as vertically integrated data sets for urban climate model evaluation. Geostationary satellites like the upcoming Sentinel-4 will enable the observation of daily cycles which will add a further dimension to study trace gas variability and to evaluate urban climate models.

Acknowledgments

We thank everyone who made this work possible. Furthermore, the authors feel obliged to thank, in advance, the readers for paying close attention.

This work was performed under the project Urban Climate Under Change [UC]^2 funded by the Federal Ministry of Education and Research (BMBF) Germany, grant number 01LP1602. Sentinel-5 Precursor is a European Space Agency (ESA) mission on behalf of the European Commission (EC). The Sentinel-5P/TROPOMI level 2 data is freely available via the Copernicus Open Access Hub (https://s5phub.copernicus.eu/). MODIS data is kindly provided by NASA (National Aeronautics and Space Administration) via the Worldview application (https://worldview.earthdata.nasa.gov), part of the Earth Observing System Data and Information System (EOSDIS). D. Klemp and R. Wegener would like to thank R. Dubus for his support with the MobiLab measurements.

References

Baumbach, G., 1996: Air Quality Control. Formation and Sources, Dispersion, Characteristics and Impact of Air Pollutants – Measuring Methods, Techniques for Reduction of Emissions and Regulations for Air Quality Control. – Berlin, Heidelberg: Springer Berlin Heidelberg (Environmental Engineering).

Baumbach, G., U. Vogt, 2003: Influence of inversion layers on the distribution of air pollutants in urban areas. – Water, Air, & Soil Pollution: Focus 3, 65–76 (2003). DOI:10.1023/A:1026098305581.

Baumüller, J. (Ed.), 2008: Klimaatlas Region Stuttgart. – Stuttgart: Verb. Region Stuttgart, Schriftenreihe/Verband Region Stuttgart, Nr. **26**.

Baumüller, J., U. Hoffmann, U. Reuter, 1998: Stadtklima 21 – Grundlagen zum Stadtklima und zur Planung "Stuttgart 21". – Landeshauptstadt Stuttgart, Amt für Umweltschutz, Abteilung Stadtklimatologie.

Bolton, D., 1980: The computation of equivalent potential temperature. – Mon. Wea. Rev. **108**, 1046–1053. DOI:10.1175/1520-0493(1980)108<1046:TCOEPT>2.0.CO;2.

Britannica, 2020: The Editors of Encyclopaedia. "temperature inversion". – Encyclopedia Britannica, 21 May. 2020, https://www.britannica.com/science/temperature-inversion (accessed at 18.07.2022).

Bukowiecki, N., J. Dommen, A.S.H. Prevot, R. Richter, E. Weingartner, U. Baltensberger, 2002: A mobile pollutant measurement laboratory-measuring gas phase and aerosol ambient concentrations with high special and temporal resolution. – Atmos. Env. **36**, 5569. DOI:10.1016/S1352-2310(02)00694-5.

Ehlers, C., 2013: Mobile Messungen – Messung und Bewertung von Verkehrsemissionen. – Dissertation, Universität zu Köln.

Erbertseder, T., H. Taubenböck, J. Meyer-Arnek, 2015: Stadtregionen als globale Zentren der Luftverschmutzung. – In: Dicke Luft – Stadtregionen als globale Zentren der Luftverschmutzung. – In: Taubenböck, H., M. Wurm, T. Esch, S. Dech (Eds): Globale Urbanisierung. Springer Spektrum, Berlin, Heidelberg. DOI:10.1007/978-3-662-44841-0_20.

Erbertseder, T., A. Roiger, A. Fiehn, T. Klausner, 2020: Evaluierung durch satelliten- und flugzeuggestützte Messungen. – Schlussbericht nach Nr. 3.2 BNBest-BMBF 98, Deutsches Fernerkundungsdatenzentrum, Deutsches Zentrum für Luft- und Raumfahrt, Oberpfaffenhofen.

European Environment Agency, 2016: Air and Health – Dispersal of air pollutants. – Published online, https://www.eea.europa.eu/publications/2599XXX/page005.html

Faragó, I., K. Georgiev, A. Havasiy, 2005: Advances in air pollution modeling for environmental security. – NATO science series **54**, Dordrecht: Springer.

Fiehn, A., J. Kostinek, M. Eckl, T. Klausner, M. Gałkowski, J. Chen, C. Gerbig, T. Röckmann, H. Maazallahi, M. Schmidt, P. Korbeń, J. Nęçki, P. Jagoda, N. Wildmann, C. Mallaun, R. Bun, A.L. Nickl, P. Jöckel, A. Fix, A. Roiger, 2020: Estimating CH_4, CO_2 and CO emissions from coal mining and industrial activities in the Upper Silesian Coal Basin using an aircraft-based mass balance approach. – Atmos. Chem. Phys. **20**, 12675–12695, DOI:10.5194/acp-20-12675-2020.

Guzmán-Torres, D., A. Eiguren-Fernández, P. Cicero-Fernández, M. Maubert-Franco, A. Retama-Hernández, R. Ramos Villegas, A.H. Miguel, 2009: Effects of meteorology on diurnal and nocturnal levels of priority polycyclic aromatic hydrocarbons and elemental and organic carbon in PM10 at a source and a receptor area in Mexico City. – Atmos. Env. **43**, 2693–2699. DOI:10.1016/j.atmosenv.2009.03.003.

Janhall, S., K. Olofson, P. Andersson, J. Pettersson, M. Hallquist, 2006: Evolution of the urban aerosol during winter temperature inversion episodes. – Atmos. Env. **40**, 5355–5366. DOI:10.1016/j.atmosenv.2006.04.051.

Kalthoff, N., B. Adler, A. Wieser, M. Kohler, K. Träumner, J. Handwerker, U. Corsmeier, S. Khodayar, D. Lambert, A. Kopmann, N. Kunka, G. Dick, M. Ramatschi, J. Wickert, C. Kottmeier, 2013: KITcube – a mobile observation platform for convection studies deployed during HyMeX. – Meteorol. Z. **22**, 633–647, DOI:10.1127/0941-2948/2013/0542.

Kampa, M., E. Castanas, 2008: Human health effects of air pollution. – Env. Poll. **151**, 362–367. DOI:10.1016/j.envpol.2007.06.012.

Khan, B., S. Banzhaf, E.C. Chan, R. Forkel, F. Kanani-Sühring, K. Ketelsen, M. Kurppa, B. Maronga, M. Mauder, S. Raasch, E. Russo, M. Schaap, M. Sühring, 2021: Development of an atmospheric chemistry model coupled to the PALM model system 6.0: Implementation and first applications. – Geosci. Model Develop. **14**, 1171–1193. DOI:10.5194/gmd-2020-286.

Kiseleva, O., B. Adler, N. Kalthoff, M. Kohler, A. Wieser, N. Wittkamp, 2019: Data set of meteorological observations (wind, temperature, humidity) collected from a microwave radiometer and lidar measurements during four intensive observations periods in 2017 and 2018 in Stuttgart, Germany, under the BMBF Program 'Urban Climate Under Change' [UC]^2). – Published online. DOI:10.5445/IR/1000093534.

Kiseleva, O., N. Kalthoff, B. Adler, M. Kossmann, A. Wieser, R. Rinke, 2022: Nocturnal atmospheric conditions and their impact on air pollutant concentrations in the city of Stuttgart. – Meteor. Appl. **28**, e2037. DOI:10.1002/met.2037.

Klemp, D., R. Wegener, R. Dubus, U. Javed, 2020: Acquisition of temporally and spatially highly resolved data sets of relevant trace substances for model development and model evaluation purposes using a mobile measuring laboratory (Vol. 497). – Jülich: Forschungszentrum Jülich GmbH, Zentralbibliothek, Verlag Jülich.

Klemp, D., R. Wegener, R. Dubus, L. Karadurmus, N. Kille, Z. Tan, 2021: Distribution of trace gases with adverse effects on fuel cells - Acquisition of temporally and spatially highly resolved data sets of relevant trace substances for model development and model evaluation purposes using a mobile measuring laboratory (Vol. 539). – Jülich: Forschungszentrum Jülich GmbH, Zentralbibliothek, Verlag Jülich.

Kolev, I., P. Savov, B. Kaprielov, O. Parvanov, V. Simeonov, 2000: Lidar observation of the nocturnal boundary layer formation over Sofia, Bulgaria. – Atmos. Env. **34**, 3223–3235. DOI: 10.1016/S1352-2310(99)00490-2.

Li, Y., M. Zhao, S. Motescharrei, Q. Mu, E. Kalnay, S. Li, 2015: Local cooling and warming effects of forests based on satellite observations. – Nat. Comm. **6**, 6603, DOI:10.1038/ncomms7603.

Lorente, A., K.F. Boersma, H.J. Eskes, J.P. Veefkind, J.H.G.M. van Geffen, M.B. de Zeeuw, H.A.C. Denier van der Gon, S. Beirle, M.C. Krol, 2019: Quantification of nitrogen oxides emissions from build-up of pollution over Paris with TROPOMI. – Sci Rep **9**, 20033. DOI:10.1038/s41598-019-56428-5.

Mabahwi, N.A.B., O.L.H. Leh, D. Omar, 2014: Human Health and Wellbeing: Human Health Effect of Air Pollution. – Procedia - Social Behavioral Sci. **153**, 221–229. DOI:10.1016/j.sbspro.2014.10.056.

Maronga, B., G. Gross, S. Raasch, S. Banzhaf, R. Forkel, W. Heldens, F. Kanani-Sühring, A. Matzarakis, M. Mauder, D. Pavlik, J. Pfafferott, S. Schubert, G. Seckmeyer, H. Sieker, K. Winderlich, 2019: Development of a new urban climate model based on the model PALM – Project overview, planned work, and first achievements. – Meteorol. Z. **28**, 105–119. DOI:10.1127/metz/2019/0909.

Maronga, B., S. Banzhaf, C. Burmeister, T. Esch, R. Forkel, D. Fröhlich, V. Fuka, K.F. Gehrke, J. Geletič, S. Giersch, T. Gronemeier, G. Gross, W. Heldens, A. Hellsten, F. Hoffmann, A. Inagaki, E. Kadasch, F. Kanani-Sühring, K. Ketelsen, B. Ali Khan, C. Knigge, H. Knoop, P. Krč, M. Kurppa, H. Maamari, A. Matzarakis, M. Mauder, M. Pallasch, D. Pavlik, J. Pfafferott, J. Resler, S. Rissmann, E. Russo, M. Salim, M. Schrempf, J. Schwenkel, G. Seckmeyer, S. Schubert, M. Sühring, R. Von Tils, L. Vollmer, S. Ward, B. Witha, H. Wurps, J. Zeidler, S. Raasch, 2020: Overview of the PALM model system 6.0. – Geosci. Model. Develop. **13**, 1335–1372. DOI: 10.5194/gmd-13-1335-2020.

Milner, J., C. Harpham, J. Taylor, M. Davies, C. Le Quéré, A. Haines, P. Wilkinson, 2019: The Challenge of Urban Heat Exposure under Climate Change: An Analysis of Cities in the Sustainable Healthy Urban Environments (SHUE) Database. – Climate **5**, 93. DOI:10.3390/cli5040093.

Müller, I., T. Erbertseder, H. Taubenböck, 2022: Tropospheric NO_2: Explorative analyses of spatial variability and impact factors. – Rem. Sens. Env. **270**, 112839, DOI:10.1016/j.rse.2021.112839.

Olofson, K.G.F., P.U. Andersson, M. Hallquist, E. Ljungström, L. Tang, D. Chen, J.B.C. Pettersson, 2009: Urban aerosol evolution and particle formation during wintertime temperature inversions. – Atmos. Env. **43**, 340–346. DOI:10.1016/j.atmosenv.2008.09.080.

Panday, A.K., R.G. Prinn, 2009: Diurnal cycle of air pollution in the Kathmandu valley, Nepal: Observations. – J. Geophys. Res. **114**, 1295. DOI:10.1029/2008JD009777.

Pérez-Invernón, F.J., H. Huntrieser, T. Erbertseder, D. Loyola, P. Valks, S. Liu, D.J. Allen, K.E. Pickering, E.J. Bucsela, P. Jöckel, J. van Geffen, H. Eskes, S. Soler, F.J. Gordillo-Vázquez, J. Lapierre, 2022: Quantification of lightning-produced NOx over the Pyrenees and the Ebro Valley by using different TROPOMI-NO_2 and cloud research products. Atmos. Meas. Tech. **15**, 3329–3351, DOI:10.5194/amt-15-3329-2022.

Samad, A., U. Vogt, 2020: Assessing the Effect of Traffic Density and Cold Airflows on the Urban Air Quality of a City with Complex Topography Using Continuous Measurements. – Modern Env. Sci. Enginer. **6**, 529–541. DOI:10.15341/mese(2333-2581)/05.06.2020/002.

Samad, A., U. Vogt, A. Panta, D. Uprety, 2020: Vertical distribution of particulate matter, black carbon and ultra-fine particles in Stuttgart, Germany. – Atmos. Poll. Res. **11**, 1441–1450. DOI: 10.1016/j.apr.2020.05.017.

Schädler, G., A. Lohmeyer, 1996: Kaltluft- und Windfeldberechnungen für Stuttgart, Heft 1, Untersuchungen zur Umwelt "Stuttgart 21". – Landeshauptstadt Stuttgart, Amt für Umweltschutz, Abteilung Stadtklimatologie.

Scherer, D., F. Antretter, S. Bender, J. Cortekar, S. Emeis, U. Fehrenbach, G. Gross, G. Halbig, J. Hasse, B. Maronga, S. Raasch, K. Scherber, 2019a: Urban Climate Under Change [UC]^2 – A National Research Programme for Developing a Building-Resolving Atmospheric Model for Entire City Regions. – Meteorol. Z. **28**, 95–104. DOI:10.1127/metz/2019/0913.

Scherer, D., F. Ament, S. Emeis, U. Fehrenbach, B. Leitl, K. Scherber, C. Schneider, U. Vogt, 2019b: Three-Dimensional Observation of Atmospheric Processes in Cities. – Meteorol. Z. **28**. 121–138. DOI:10.1127/metz/2019/0911.

Schnitzhofer, R., M. Norman, A. Wisthaler, J. Vergeiner, F. Harnisch, A. Gohm, F. Obleitner, A. Fix, B. Neininger, A. Hansel, 2009: A multimethodological approach to study the spatial distribution of air pollution in an Alpine valley during wintertime. – Atmos. Chem. Phys. **9**, 3385 – 3396. DOI:10.5194/acp-9-3385-2009.

Silva, P.J., E.L. Vawdrey, M. Corbett, M. Erupe, 2007: Fine particle concentrations and composition during wintertime inversions in Logan, Utah, USA. – Atmos. Env. **41**, 5410–5422. DOI: 10.1016/j.atmosenv.2007.02.016.

Spronken-Smith, R.A., T.R. Oke, 1999: Scale modelling of nocturnal cooling in urban parks. – Bound.-Layer Meteor. **93**, 287–312.

United Nations, 2018: World Urbanization Prospects 2018. – United Nations (UN), https://population.un.org/wup/

Van Geffen, J.H.G.M., H.J. Eskes, K.F. Boersma, J.D. Maasakkers, J.P. Veefkind, 2019: TROPOMI ATBD of the total and tropospheric NO_2 data products. – Published online, https://sentinel.esa.int/documents/247904/2476257/Sentinel‑5P-TROPOMI-ATBD-NO2-data-products (accessed at 16.03.2021).

Van Geffen, J., H. Eskes, S. Compernolle, G. Pinardi, T. Verhoelst, J.-C. Lambert, M. Sneep, M. ter Linden, A. Ludewig, K.F. Boersma, J.P. Veefkind, 2022: Sentinel-5P TROPOMI NO_2 retrieval: impact of version v2.2 improvements and comparisons with OMI and ground-based data. – Atmos. Meas. Tech. **15**, 2037–2060, DOI:10.5194/amt-15-2037-2022.

Veefkind, J.P., I. Aben, K. McMullan, H. Förster, J. de Vries, G. Otter, J. Claas, H.J. Eskes, J.F. de Haan, Q. Kleipool, M. van Weele, O. Hasekamp, R. Hoogeveen, J. Landgraf, R. Snel, P. Tol, P. Ingmann, R. Voors, B. Kruizinga, R. Vink, H. Visser, P.F. Levelt, 2012: TROPOMI on the ESA Sentinel-5 Precursor: A GMES mission for global observations of the atmospheric composition for climate, air quality and ozone layer applications. – Rem. Sens. Env. **120**, 70–83. DOI:10.1016/j.rse.2011.09.027.

Vogt, U., G. Baumbach, S. Hansen, 1999: Messungen der Kaltluftströme und Luftverunreinigungs-Vertikalprofile im Plangebiet "Stuttgart 21". – Landeshauptstadt Stuttgart, Amt

für Umweltschutz, Abteilung Stadtklimatologie, https://www.stadtklima-stuttgart.de/index.php?klima_s21_themenhefte_h15

Voigt, C., J. Lelieveld, H. Schlager, J. Schneider, J. Curtius, R. Meerkötter, D. Sauer, L. Bugliaro, B. Bohn, J.N. Crowley, T. Erbertseder, S. Gross, V. Hahn, Q. Li, M. Mertens, M.L. Pöhlker, A. Pozzer, U. Schumann, L. Tomsche, J. Williams, A. Zahn, M. Andreae, S. Borrmann, T. Bräuer, R. Dörich, A. Dörnbrack, A. Edtbauer, L. Ernle, H. Fischer, A. Giez, M. Granzin, V. Grewe, H Harder, M. Heinritzi, B.A. Holanda, P. Jöckel, K. Kaiser, O.O. Krüger, J. Lucke, A. Marsing, A. Martin, S. Matthes, C. Pöhlker, U. Pöschl, S. Reifenberg, A. Ringsdorf, M. Scheibe, I. Tadic, M. Zauner-Wieczorek, R. Henke, M. Rapp, 2022: Cleaner skies during the COVID-19 lockdown. – Bull. Amer. Meteor. Soc. **103**, E1796–E1827, DOI:10.1175/BAMS-D-21-0012.1.

Weijers, E.P., A.Y. Khlystov, G.P.A. Kos, J.M. Erishmen, 2004: Variability of particulate matter concentrations along roads and motorways determined by a moving measurement unit. Atmos. Env. **38**, 2993. DOI:10.1016/j.atmosenv.2004.02.045.

Westerdahl, D., S. Fruin, T. Sax, P.M. Fine, C. Sioutas, 2005: Mobile platform measurements of ultrafine particle and associated pollutant concentrations on freeways and residential streets in Los Angeles. Atmos. Env. **39**, 3597. DOI:10.1016/j.atmosenv.2005.02.034.

Wittkamp, N., B. Adler, N. Kalthoff, O. Kiseleva, 2021: Mesoscale wind patterns over the complex urban terrain around Stuttgart investigated with dual-Doppler Lidar profiles. – Meteorol. Z. **30**, 185–200. DOI:10.1127/metz/2020/1029.

World Health Organisation (WHO), 2021: Fact Sheet, Ambient (outdoor) air pollution. Published online, https://www.who.int/news-room/fact-sheets/detail/ambient-(outdoor)-air-quality-and-health (accessed at 16.08.2022).

Yamazaki, D., D. Ikeshima, R. Tawatari, T. Yamaguchi, F. O'Loughlin, J.C. Neal, C.C. Sampson, S. Kanae, P.D. Bates, 2017: A high accuracy map of global terrain elevations. – Geophys. Res. Lett. **44**, 5844–5853. DOI:10.1002/2017GL072874.

Yan, H., F. Wu, L. Dong, 2018: Influence of a large urban park on the local urban thermal environment. – Sci. Total Env. **622–623**, 882–891, DOI:10.1016/j.scitotenv.2017.11.327.

Zeeman, M., C.C. Holst, M. Kossmann, D. Leukauf, C. Münkel, A. Philipp, R. Rinke, S. Emeis, 2022: Urban Atmospheric Boundary-Layer Structure in Complex Topography: An Empirical 3D Case Study for Stuttgart, Germany. – Front. Earth Sci. **10**, 840112. DOI:10.3389/feart.2022.84011.

Zoras, S., A.G. Triantafyllou, D. Deligiorgi, 2006: Atmospheric stability and PM10 concentrations at far distance from elevated point sources in complex terrain: worst-case episode study. – J. Env. Manag. **80**, 295–302. DOI:10.1016/j.jenvman.2005.09.010.